The paleobiology and paleoecology of South African *Lystrosaurus*

Jennifer Botha

Department of Karoo Palaeontology, National Museum, Bloemfontein, Free State, South Africa
Department of Zoology and Entomology, University of the Free State, Bloemfontein, Free State, South Africa

ABSTRACT

Lystrosaurus was one of the few tetrapods to survive the end-Permian mass extinction (EPME), the most catastrophic biotic crisis in Phanerozoic history. The significant increased abundance of this genus during the post-extinction Early Triassic recovery period has made *Lystrosaurus* an iconic survivor taxon globally and ideal for studying changes in growth dynamics during a mass extinction. There is potential evidence of a Lilliput effect in *Lystrosaurus* in South Africa as the two Triassic species that became highly abundant after the EPME are relatively smaller than the two Permian species. In order to test this hypothesis a detailed examination of the body size and life history of Permo-Triassic *Lystrosaurus* is required. In this study, the basal skull length and growth patterns of the four South African *Lystrosaurus* species from the Karoo Basin, *L. maccaigi*, *L. curvatus*, *L. murrayi* and *L. declivis*, were examined using cranial measurements and bone histology. The basal skull length measurements show that the Triassic species are smaller than the Permian species and supports previous studies. The osteohistology examination of all four species reveal rapidly forming fibrolamellar bone tissues during early to mid-ontogeny. Growth marks are common in *L. maccaigi* and *L. curvatus*, but rare and inconsistent in the purely Triassic *L. murrayi* and *L. declivis*. The inconsistency of the growth marks in these latter two taxa suggests the presence of developmental plasticity. This feature may have been advantageous in allowing these species to alter their growth patterns in response to environmental cues in the post-extinction Early Triassic climate. An overall transition to slower forming parallel-fibered bone is observed in the largest individuals of *L. maccaigi*, but absent from the limb bones of the other species. The absence of such bone tissue or outer circumferential lamellae in *L. curvatus*, *L. murrayi* and *L. declivis* indicates that even the largest collected specimens do not represent fully grown individuals. Although *L. murrayi* and *L. declivis* are smaller in size, the lack of a growth asymptote in the largest specimens indicates that adult individuals would have been notably larger and may have been similar in size to large *L. maccaigi* and *L. curvatus* when fully grown. Thus, the previously described Lilliput effect, recognized by some authors in the Karoo fossil record (such as the therocephalian *Moschorhinus kitchingi*), may be a product of high juvenile excess mortality in the Triassic rather than a strict "dwarfing" of *Lystrosaurus* species. The lifestyle of *Lystrosaurus* was also re-examined. Although previous studies have proposed an aquatic lifestyle for the genus, the similar morphology and bone microanatomy to several other large terrestrial Permo-Triassic dicynodonts supports a fully terrestrial mode of life.

Corresponding author
Jennifer Botha, jbotha@nasmus.co.za

INTRODUCTION

The "Lilliput effect" was first defined by *Urbanek (1993)* to describe reduced body sizes in organisms living through unfavorable growing conditions during a mass extinction. The term has since been expanded to include a number of patterns such as the preferential survival of smaller taxa (faunal sorting), dwarfing within a single species, and size reduction amongst a variety of clades that includes notable morphological change (miniaturization) (*Harries & Knorr, 2009*). The Lilliput effect has been reported in a variety of marine invertebrates such as Early Silurian corals (*Kaljo, 1996*), Late Devonian conodonts (*Renaud & Girard, 1999*) and Early Danian echinoids (*Jeffery, 2001*). It has been less documented amongst terrestrial taxa, but decreased body sizes have been seen in land vertebrates across the K-T boundary (*Buffetaut, 2006*) and amongst the Pleistocene megafaunal extinctions (*Brook & Bowman, 2002*).

The end-Permian mass extinction (EPME) is widely regarded as the most catastrophic of the five Phanerozoic mass extinctions in Earth's history (*Erwin, Bowring & Yugan, 2002*; *Irmis & Whiteside, 2012*; *Benton & Newell, 2014*). Current estimations from the marine Global Boundary Stratotype Section and Point at Meishan, China indicate that the main event took place approximately 251.9 million years ago (Ma) (*Burgess, Bowring & Shen, 2014*). Proposed mechanisms of the extinction include global warming, atmospheric hypoxia (decreased oxygen levels), oceanic anoxia associated with hypercapnia (increased carbon dioxide levels) and/or euxinia (increased sulphide levels) (*Wignall & Twitchett, 1996*; *Knoll et al., 1996*; *Isozaki, 1997*; *Hotinski et al., 2001*; *Kump, Pavlov & Arthur, 2005*), excessive methane release (*Krull et al., 2000*; *Sheldon & Retallack, 2002*), increased mercury levels (*Shen et al., 2019*) and regional terrestrial aridification (*Ward, Montgomery & Smith, 2000*; *Ward et al., 2005*; *Smith & Ward, 2001*). Siberian Trap volcanism is currently the most widely proposed driving force behind the extinction, which is thought to have triggered the release of massive amounts of methane, sulphur dioxide and carbon dioxide into the atmosphere (*Wignall, 2001*; *Benton & Twitchett, 2003*; *Erwin, 2006*; *Knoll et al., 2007*; *Algeo et al., 2011*; *Shen et al., 2011*; *Payne & Clapham, 2012*; *Retallack, 2013*).

The EPME had a considerable effect on both marine and terrestrial ecosystems, substantially changing community structure, causing a severe reduction in global biodiversity (*Xie et al., 2005*; *Yin et al., 2007*; *Shen et al., 2011*; *Chen & Benton, 2012*; *Smith & Botha-Brink, 2014*; *Roopnarine & Angielczyk, 2015*; *Roopnarine et al., 2018*; *Roopnarine et al., 2019*). In the South African Karoo Basin, where the terrestrial aspect of the extinction is best preserved, the post-extinction environment has been described as unpredictable, with increased aridity and temperature extremes (*Smith & Botha, 2005*; *Smith & Botha-Brink, 2014*; *Rey et al., 2016*; *MacLeod, Quinton & Bassett, 2017*; *Botha et al., 2020*) (although see *Gastaldo et al., 2020* for proposed seasonally wet conditions during the latest Permian). Species survival was variable, with some going extinct (e.g., pareiasaurian

parareptiles, gorgonopsian therapsids), others surviving for a time at reduced diversity levels (e.g., dicynodont and therocephalian therapsids) and others radiating after the EPME to become particularly diverse during the Triassic (e.g., temnospondyl amphibians, procolophonid parareptiles, archosauromorph reptiles and cynodont therapsids) (*Ruta & Benton, 2008*; *Nesbitt et al., 2013*; *Ruta et al., 2013a*; *Ruta et al., 2013b*; *MacDougall, Brocklehurst & Fröbisch, 2019*). Two recent studies have shown that there is still controversy regarding the position of the terrestrial Permo-Triassic boundary (PTB) in the South African Karoo Basin (*Botha et al., 2020*; *Gastaldo et al., 2020*). Based on *Gastaldo et al. (2020)* the upper Palingkloof Member of the Balfour Formation, which contains the PTB in the main Karoo Basin, is no older than 252.24 ± 0.1 Ma, which would suggest a Permian age. However, it may be as young as 251.7 ± 0.3 Ma based on the identification of even younger detrital zircon populations below this interval (*Botha et al., 2020*). This most likely places the base of the *Lystrosaurus declivis* Assemblage Zone within the basal Triassic as in the *Lystrosaurus murrayi*-dominated fauna of India's Panchet beds (*Tripathi & Puri, 1962*; *Tripathi & Satsangi, 1963*) consistent with the currently accepted position of the PTB interval in the main Karoo Basin (e.g., *Smith & Ward, 2001*; *Smith & Botha-Brink, 2014*; *Botha et al., 2020*). The placement of the PTB in the Karoo Basin in this study is placed according to *Botha et al. (2020)* (i.e., the 'traditional' placement) and not according to the *Gastaldo et al. (2020)* alternative higher in the section.

A Lilliput effect across the EPME in the marine realm has been reported for a variety of taxa (*Twitchett, 2007*) including conodonts (*Luo et al., 2008*), bivalves, gastropods, brachiopods (*Metcalfe, Twitchett & Price-Lloyd, 2011*) and foraminifera (*Song, Tong & Chen, 2011*). Fewer studies have documented such an effect in the terrestrial realm. However, studies on South African therocephalian synapsids have reported post-extinction body size reductions in the form of within-lineage heterochronic shifts (dwarfism in *Moschorhinus kitchingi*) and the differential survival of some small-bodied therocephalians (e.g., baurioids) (*Huttenlocker & Botha-Brink, 2013*; *Huttenlocker & Botha-Brink, 2014*). Amongst anomodont dicynodonts large taxa disappeared across the PTB only to reappear later during the Middle Triassic (*Angielczyk & Walsh, 2008*).

One of the few tetrapod species that survived the EPME is the well-known dicynodont therapsid *Lystrosaurus*. It is the only dicynodont found on either side of the PTB and constitutes more than 90% of the vertebrate fauna from the Early Triassic *Lystrosaurus declivis* Assemblage Zone (*Botha & Smith, 2020*). Although relatively rare during the Late Permian, the Early Triassic species inundated post-extinction communities to become the dominant tetrapods in terrestrial ecosystems after the EPME (*Smith, Rubidge & Van der Walt, 2012*; *Botha-Brink, Huttenlocker & Modesto, 2014*). In the South African Karoo Basin, the biostratigraphy of the four *Lystrosaurus* species, which comprise *L. maccaigi*, *L. curvatus*, *L. murrayi* and *L. declivis* (*Grine et al., 2006*; *Botha & Smith, 2007*), is well-documented (*Botha & Smith, 2007*; *Botha et al., 2020*). Until recently, *L. curvatus* was the only South African species to be found on both sides of the PTB (sensu *Botha et al., 2020*), with *L. maccaigi* disappearing at the PTB and *L. murrayi* and *L. declivis* being found in purely Triassic deposits (*Botha & Smith, 2007*; *Smith & Botha-Brink, 2014*). However, a recent study on a relatively new PTB site has revealed that *L. maccaigi* once
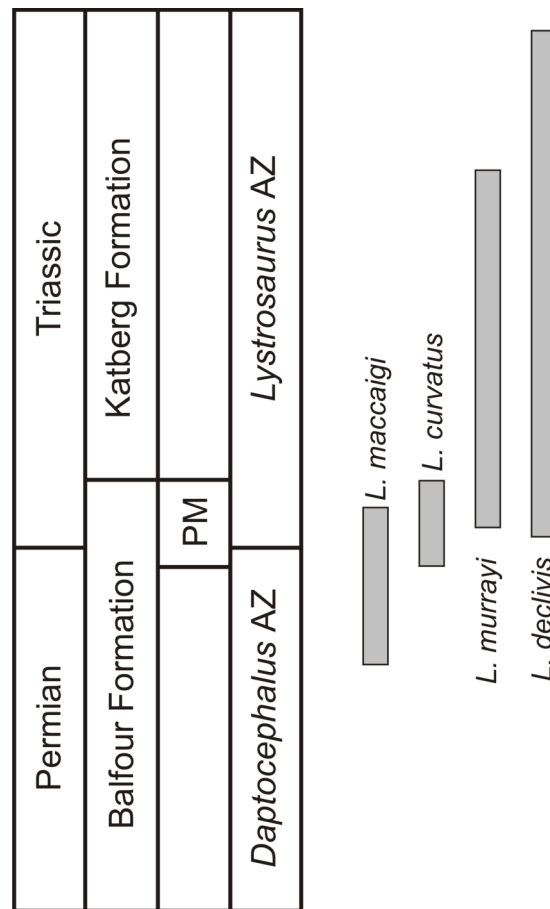
Figure 1 Biostratigraphic ranges of the four South African *Lystrosaurus* species in the Karoo Basin.
Abbreviations: AZ, Assemblage Zone; PM, Palingkloof Member.

considered to be solely Permian in South Africa also crossed the boundary (*Botha et al., 2020*). This is not unexpected as *L. maccaigi* was found in Triassic strata of the Fremouw Formation in Antarctica during the 1980s (*Cosgriff, Hammer & Ryan, 1982*). Both *L. maccaigi* and *L. curvatus* disappear in the Triassic portion of the Palingkloof Member, Balfour Formation and have yet to be found in the overlying Katberg Formation of the *Lystrosaurus declivis* Assemblage Zone (*Botha et al., 2020*; *Botha & Smith, 2020*), whereas the ranges of *L. murrayi* and *L. declivis* continue into the Katberg Formation, with *L. declivis* being found through to the top of the *Lystrosaurus declivis* Assemblage Zone (*Botha & Smith, 2006*; *Botha & Smith, 2020*) (Fig. 1). The purely Triassic species, *L. murrayi* and *L. declivis*, are considered to have had smaller body sizes compared to the Permian originating species, *L. maccaigi* and *L. curvatus* (*Grine et al., 2006*) providing possible evidence for a Lilliput effect in this genus. The excellent biostratigraphical resolution of *Lystrosaurus* makes it possible to assess the presence of such a pattern in this genus, i.e., was there a dwarfing of *Lystrosaurus* during the EPME?

The history of *Lystrosaurus* osteohistology

An excellent method for assessing life history patterns in extinct animals is the examination of their bone histology or osteohistology. The microstructure of fossil bone records important information about the life history of an extinct vertebrate. These data include ontogenetic, growth, lifestyle and biomechanical information, which would otherwise not be accessible using more traditional methods. The osteohistology of *Lystrosaurus* was first examined by *Ricqlès (1972)*, *Ricqlès (1976)*, and *Ricqlès et al. (1991)* who examined isolated fragments of humeri and tibiae, as well as *Chinsamy & Rubidge (1993)* who also briefly assessed a humerus of *L. murrayi*. More recently, *Ray, Chinsamy & Bandyopadhyay (2005)* provided a comprehensive assessment of the ontogeny of *L. murrayi* (reassessed in *Ray, Bandyopadhyay & Bhawal, 2009*), and *Botha-Brink & Angielczyk (2010)* briefly compared the bone tissue patterns of *L. maccaigi*, *L. murrayi* and *L. declivis*. However, none of these studies comprised a comprehensive ontogenetic comparison between the Permian and Triassic species. *Botha-Brink & Angielczyk (2010)* and more recently *Botha-Brink et al. (2016)* hypothesized that the high degree of vascularization observed in Triassic *Lystrosaurus* facilitated rapid growth in these species, which may have aided in their survival during this time. However, a more rigorous examination by quantifying Permian and Triassic *Lystrosaurus* life history patterns is required to test this hypothesis. Additionally, *Ray, Chinsamy & Bandyopadhyay (2005)* provided an alternative hypothesis for its survivorship suggesting that Triassic *Lystrosaurus* was semi-aquatic. This has been a persistent hypothesis since Broom first proposed it in 1902. Consequently, *Jasinoski & Chinsamy-Turan (2012)* suggested that the abundance of vascular canals was not related to growth rate, but rather increased porosity in Triassic *Lystrosaurus* limb bones. Increased porosity in extant pelagic aquatic mammals has been found to lighten the skeleton and thus, may counteract buoyancy while in the water (*Wall, 1983*).

As Permo-Triassic *Lystrosaurus* formed such an important part of the ecosystems associated with the EPME and as the lifestyle of this genus remains controversial, the aim of this study is to comprehensively examine changes in body size, bone microanatomy and osteohistology of the four South African *Lystrosaurus* species in order to quantify their life history patterns during the EPME and test the semi-aquatic hypothesis and whether it played a role in *Lystrosaurus* survivorship.

METHODS

Seventy seven limb bones and ribs from 38 individuals of the four South African *Lystrosaurus* species were examined (Table S1). Elements were identified to species level based on the presence of skull material (according to *Grine et al., 2006*; *Botha & Smith, 2007*). Limb bones were purposely selected because they document the most complete growth record of the animal. The mid-diaphysis undergoes the least secondary remodeling and thus, elements were thin sectioned in this region wherever possible (*Chinsamy, 1990*; *Chinsamy, 1991*; *Chinsamy, 1995*; *Francillon-Vieillot et al., 1990*; *Horner, de & Padian, 1999*). However, as recent studies have found that additional information regarding collagen fibril organisation can be obtained from longitudinal sections and are thus helpful in confirming initial

observations from transverse sections, longitudinal sections of the diaphyseal/metaphyseal regions (as the mid-diaphysis was left for transverse sectioning) were also made when possible (*Stein & Prondvai, 2014*). Elements were only taken from specimens that could be identified to species level.

A database from containing 259 measurements of *Lystrosaurus* basal skull length (BSL) was used to develop a growth distribution for each species (Table S2). For each specimen, the ontogenetic stage or age class was estimated by calculating the BSL as a percentage of the maximum BSL available for the relevant species (389 mm for *L. maccaigi*, 246 mm for *L. curvatus*, 213 mm for *L. murrayi*, and 226 mm for *L. declivis*). Individuals were divided into four age classes based on this database; Age Class I represents juveniles of less than 40% of the maximum known size (MKS) for each particular species; Age Class II represents early subadults of 40–59% MKS; Age Class III represents late subadults of 60–79% MKS and Age Class IV represents adults of 80–100% MKS (after *Botha-Brink et al., 2016*).

Thin sectioning was conducted at the National Museum, Bloemfontein using standard techniques following that set out in *Gower et al. (2014)* and *Ecker et al. (2015)*. Each element was embedded in a clear epoxy resin Struers Epofix, to prevent the bones from disintegrating during the thin sectioning process. The embedding was completed within a Struers CitoVac vacuum chamber to remove air bubbles from within the bone and surrounding resin. The resin was left to cure for 24 h and then sequential transverse sections of the midshaft of each element (and when possible longitudinal sections of the diaphyseal/metaphyseal regions), approximately 1.5 mm thick, were cut using a cut-off diamond-tipped saw within a Struers Accutom-50 cut-off grinding machine. Each section was then mounted onto a frosted petrographic glass slide using the resin adhesive LR20, which had been placed in the Struers CitoVac vacuum chamber to remove air bubbles. Pressure was then applied to the sections to eliminate any excess bubbles. Once set, the sections were ground to approximately 60 μm thick (although the thickness varied between elements, due to variable preservation of each bone) using a diamond-tipped grinding wheel within the Struers Accutom-50 cut-off grinding machine. The resulting thin sections were polished until smooth using a Struers LaboPol 5 polishing machine (*Gower et al., 2014*; *Ecker et al., 2015*). The bone microstructure was viewed and photographed using a Nikon Eclipse 50i Polarizing microscope and DS-Fi1 digital camera and captured in the computer program NIS Elements D 4.6 (Nikon Corp., Tokyo, Japan). Osteohistology terminology follows that of *Francillon-Vieillot et al. (1990)*, *Ricqlès et al. (1991)* and *Stein & Prondvai (2014)*.

The thickness of the cortex and the overall compactness of the bone of the largest histologically-sampled individuals of each species were measured in order to assess the robustness of the bones and to make inferences regarding lifestyle (Figs. 2A–2K) as described by *Gower et al. (2014)*. The midshaft cortical thickness (k, expressed from 0 to 1 where cortical thickness is thickest when k tends towards 0, (*Currey & Alexander, 1985*)) was recorded for the limb bones by measuring the ratio between the inner diameter and outer diameter of the bone in the computer program Bone Profiler for Windows V4.5.8 (*Girondot & Laurin, 2003*). A bone compactness profile (defined as "the ratio between the surface occupied by bone tissues and the total bone surface", (*Germain & Laurin, 2005*:337) was also obtained from the midshaft of each element also using Bone Profiler
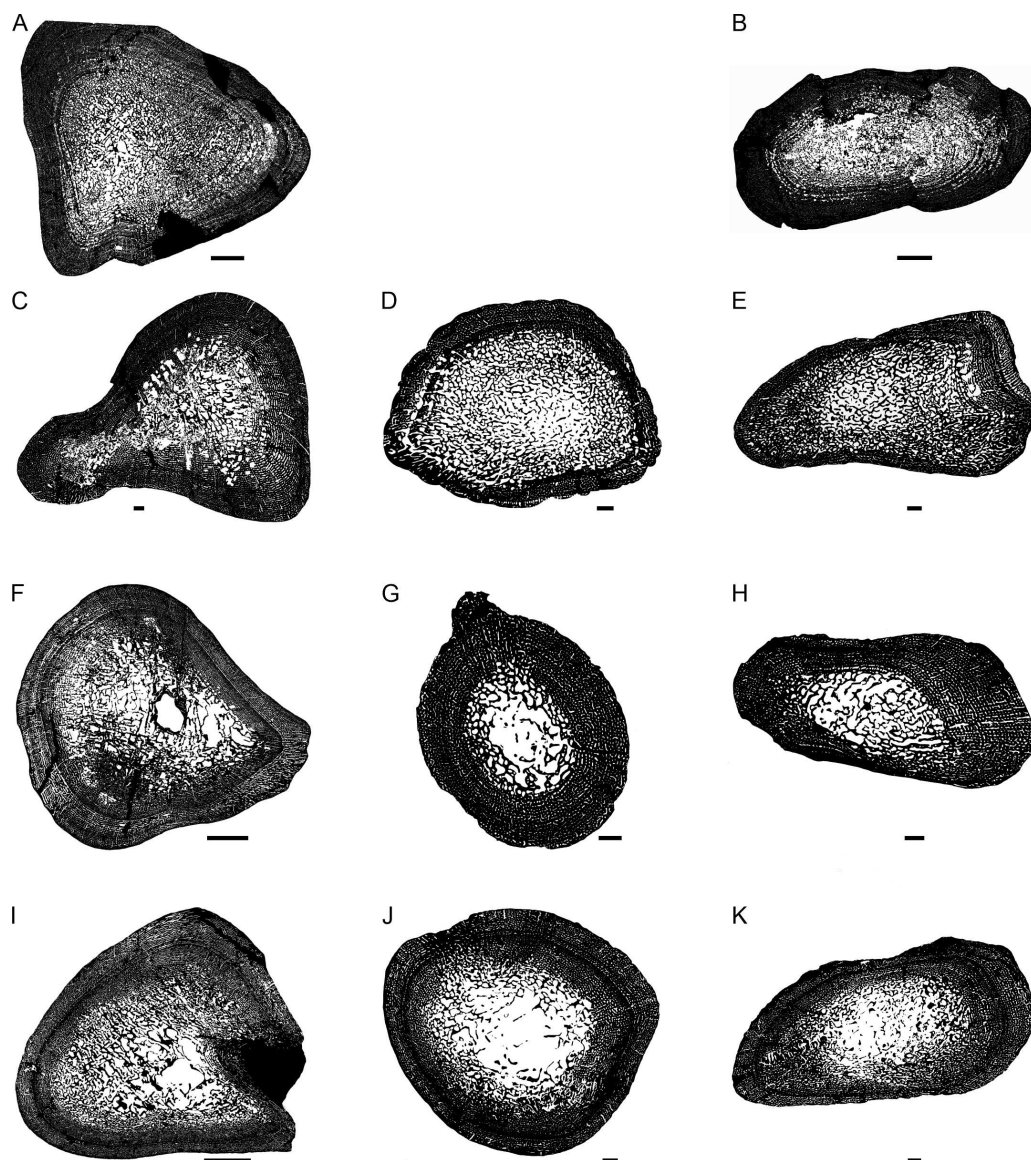
Figure 2   Transverse sections of the largest specimens of the South African *Lystrosaurus* species, used to assess the bone microanatomy. (A) *L. maccaigi* NMQR 3663a humerus. (B) *L. maccaigi* NMQR 3663b ulna. (C) *L. curvatus* NMQR 3922a humerus. (D) *L. curvatus* NMQR 3651b radius. (E) *L. curvatus* NMQR 3651c ulna. (F) *L. murrayi* BP/1/3236 humerus. (G) *L. murrayi* NMQR 659b radius. (H) *L. murrayi* NMQR 659c ulna. (I) *L. declivis* NMQR 1485a humerus. (J) *L. declivis* NMQR 1485b radius. (K) *L. declivis* NMQR 1485c ulna. Scale bars equal 1,000 μm, apart from A, B and I which equal 5,000 μm.

for Windows. This profile or global compactness (Cg) represents the ratio between the mineralized tissue surface and the total cross-sectional surface and is higher towards a value of 1 (*Girondot & Laurin, 2003*; *Laurin, Girondot & Loth, 2004*; *Germain & Laurin, 2005*; *Canoville & Laurin, 2010*). Global compactness, Cc (bone center compactness), Cp (bone periphery compactness), Min (minimum compactness), Max (maximum compactness), S (proportional to the width of the transition zone from medullary cavity to cortex) and

P (the transition area from medullary cavity to cortex) were used to predict a lifestyle for the humerus (*Canoville & Laurin, 2010*) and radius (*Laurin, Canoville & Germain, 2011*). Although there is currently no formula for predicting lifestyle in the ulna, K and Cg were also measured in order to make comparisons between the *Lystrosaurus* species as well as with extant taxa.

The relative vascular area in the primary cortex was measured using the Nikon software NIS elements D 4.6 (Nikon Corp., Tokyo, Japan). As the organization and density of the vascular canals in the primary cortex is closely related to bone deposition rate (e.g., *Amprino, 1947*; *Margerie & Castanet, 2002*; *Margerie et al., 2004*), this method provides a quantitative way for comparing between different elements and taxa. The maximum possible vascularization for each element is quantified because the vascular canals would have included lymph and nerves as well as blood vessels during life (*Starck & Chinsamy, 2002*). Cortical vascularity was calculated by randomly selecting ten standardized quadrants from the midcortex of each section (thus excluding areas of secondary remodeling). The total canal area was calculated and divided by the total cortical area and then multiplied by 100 to obtain a percentage (Table S1). Mean primary osteon diameter also reflects bone apposition rates and is generally highest in highly woven fibrolamellar bone (*Margerie & Castanet, 2002*). Mean primary osteon diameter was calculated (in microns) by measuring the transverse widths of primary osteons in the cortex under polarized light (Table S1).

RESULTS

Osteohistology

L. maccaigi

Age Class I (<40%)— Two individuals comprising a humerus, radius (NMQR 3658) and tibia (NMQR 3641) were available for study (Table S1). NMQR 3658 (Fig. 3A) was recovered from Permian deposits whereas NMQR 3641 (Fig. 3B) was recovered from Triassic deposits. Individuals in this ontogenetic stage contain medullary cavities that are infilled by a labyrinth of bony trabeculae (Fig. 3A) or are tiny (Fig. 3B). The perimedullary cancellous bone tissue transforms gradually into a thick compact cortex, which comprises highly vascularized (mean cortical vascularity 13.5%) fibrolamellar bone tissue. The fibrolamellar complex is identified as such by the presence of a woven-fibered interstitial matrix (distinguished by the woven-fibered texture and disorganized non-lamellar nature of the matrix) containing numerous haphazardly-arranged globular osteocyte lacunae and the random arrangement of longitudinally-arranged primary osteons (mean diameter 83 μm) (Figs. 3C–3F). The presence of such bone tissue indicates rapid growth as both woven-fibered bone and high cortical vascularity are linked to rapid bone apposition rates (*Amprino, 1947*; *Margerie & Castanet, 2002*; *Margerie et al., 2004*). The vascular canals decrease in size slightly on one side of the bone in NMQR 3641. Secondary osteons are small and rare, and limited to the peri-medullary region. Growth marks in the form of annuli or Lines of Arrested Growth (LAG) are absent from both individuals (Figs. 3A–3F). These marks indicate a temporary decrease (annuli) or cessation (LAGs) in bone growth and are deposited annually in extant vertebrates (*Hutton, 1986*). Sharpey's fibers indicating
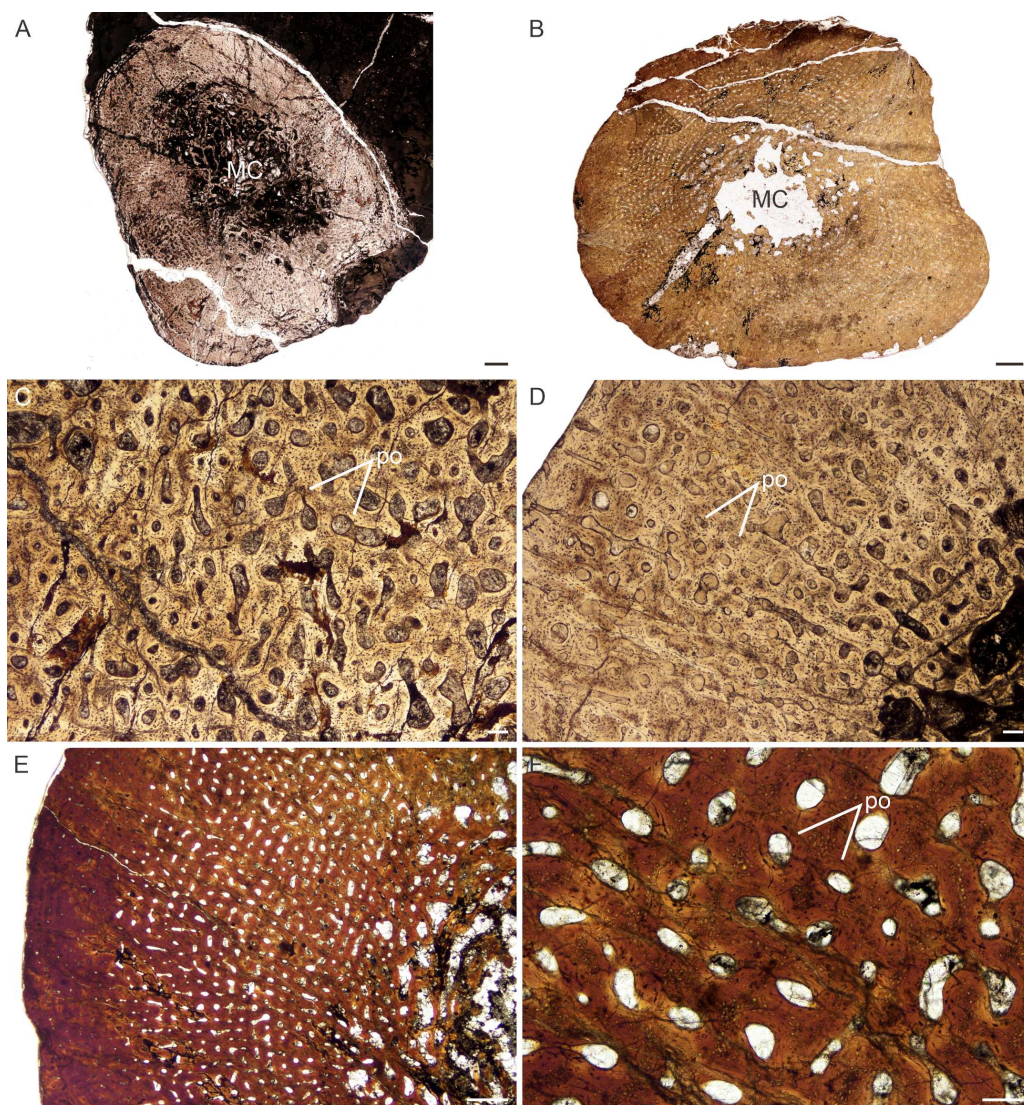
Figure 3 **Transverse sections of the bone histology of *Lystrosaurus maccaigi*, Age Class I.** (A) NMQR 3658a humerus showing an infilled medullary cavity. (B) NMQR 3641 tibia showing a thick cortex surrounding a small medullary cavity. (C) NMQR 3658a humerus showing woven fibered bone with primary osteons. (D) NMQR 3658b radius showing highly vascularized primary bone tissue. (E) NMQR 3641 tibia showing highly vascularized primary bone tissue. (F) High magnification of NMQR 3641 tibia showing the primary osteons. Abbreviations: MC, medullary cavity; PO, primary osteons. Scale bars equal 100 μm, apart from E, which equals 500 μm and A and B, which equal 1,000 μm.

areas of muscle or tendonous insertion were observed in the deltopectoral crest region of humerus NMQR 3658a, on the lateral side of radius NMQR 3658b as well as the posterior side of tibia NMQR 3641.

Age Class II (40%–59%)— Four individuals including a humerus, femur, tibiae, fibula and rib were available for assessment (Table S1). NMQR 796 (Fig. 4A) and SAM-PK-K10571 were recovered from Permian deposits whereas NMQR 4095 (Fig. 4B) and NMQR
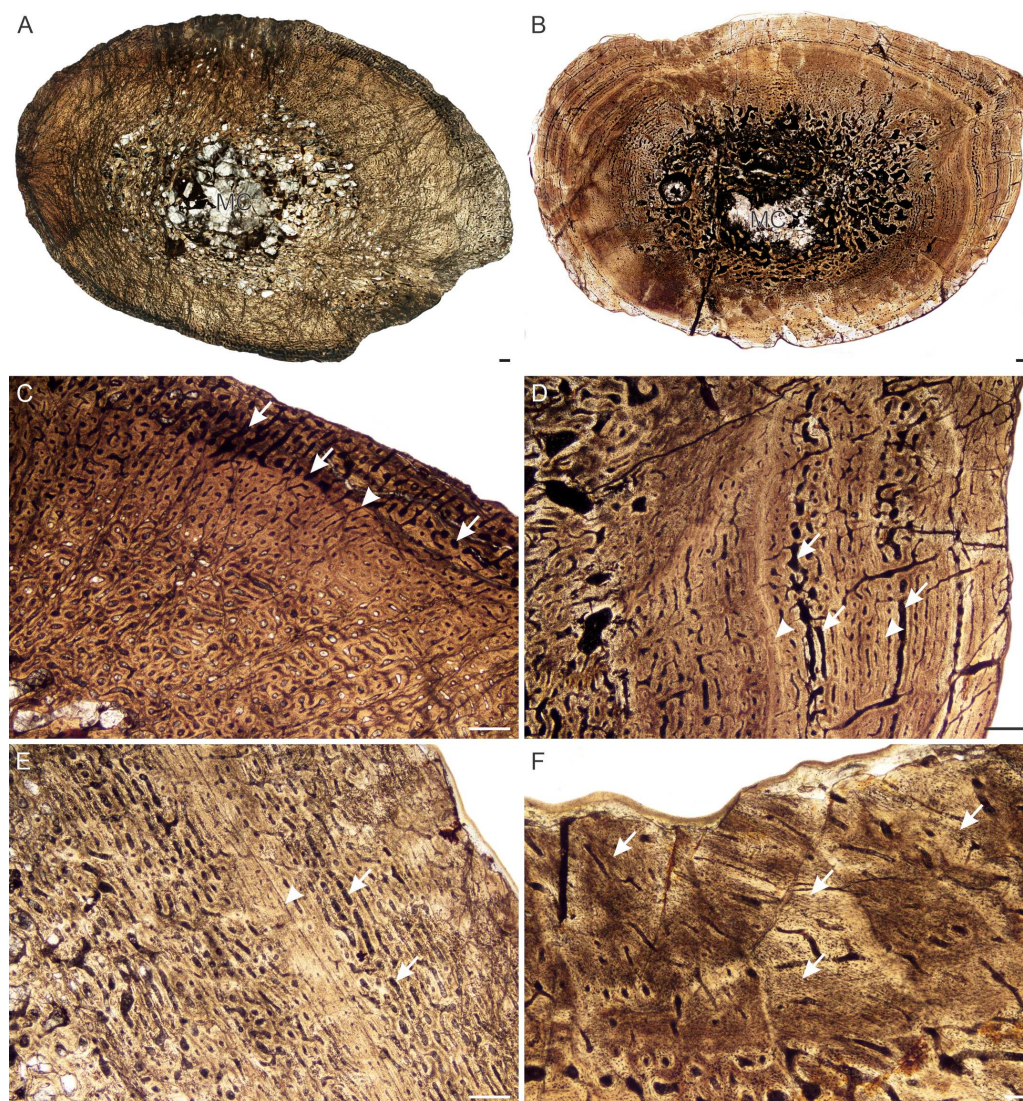
Figure 4 Transverse sections of the bone histology of *Lystrosaurus maccaigi*, Age Class II. (A) NMQR 796a tibia showing an infilled medullary cavity. (B) NMQR 4095 femur showing a gradual transition from medullary cavity to compact cortex. (C) NMQR 796a tibia showing enlarged canals (arrows) and an annulus (arrowhead). (D) NMQR 4095 femur showing enlarged canals (arrows) and two annuli (arrowheads). (E) NMQR 3648 humerus showing large canals (arrows) and a LAG (arrow). (F) NMQR 4095 femur showing Sharpey's fibers (arrows). Scale bars equal 500 µm, apart from F, which equals 100 µm.

3648 were recovered from Triassic deposits. The medullary cavities are almost completely infilled with trabecular bone, with a few elements having tiny open medullary cavities. The compact cortex is relatively thick. The bone tissues remain similar to those individuals from Stage Class I. However, growth marks in the form of annuli and LAGs are present in all individuals ranging from one to three growth marks (Figs. 4C–4F). In tibia NMQR 796a (47% MKS) a region of relatively small vascular canals is followed by a region of enlarged vascular canals (Fig. 4C). Although a growth mark was not observed separating

the two regions, the clear difference suggests some form of cyclicity. I interpret the change in vascular canal size to represent a change in season similar to what a growth mark would represent (Table S1). Similar enlarged vascular canals were found in femur NMQR 4095 (Fig. 4D) and humerus NMQR 3648 (Fig. 4E) associated with annuli. These canals form reticular and laminar networks. They are primary in nature (mean diameter 78 μm) and do not exhibit any characteristics that would suggest they are secondary (e.g., Howship's lacunae, cement line, overlapping). Secondary osteons are small, isolated and limited to the inner cortex. Sharpey's fibers were observed in femur NMQR 4095 (Fig. 4F) on the posterior surface possibly for the insertion of M. coccygeo-femoris (*Ray, 2006*).

Age Class III (60%–79%)— Four individuals including humeri, femora and a tibia were available for study (Figs. 5A–5F). One individual, NMQR 3689, was recovered from Triassic deposits, the rest are from Permian deposits (Table S1). The medullary cavities are almost completely infilled with a generally gradual transition zone from cavity to compact cortex (Figs. 2A, Figs. 2B, 5A, 5B). The cortex continues to be dominated by fibrolamellar bone with vascular canals in a laminar longitudinally-oriented network. The smallest individual in this age class, NMQR 3689 (Fig. 5C), is highly vascularized (mean cortical vascularity 16%, Table S1) with large primary vascular canals (mean diameter 78 μm, Table S1). The largest elements have slightly smaller vascular canals (mean primary osteon diameter 71 μm, Table S1) and the bone tissue becomes parallel-fibered from the mid-cortex (e.g., NMQR 3663, Fig. 5D). Secondary osteons are rare in NMQR 3689, but become increasingly prevalent in the larger elements. Secondary resorption is extensive, with resorption cavities extending into the mid-cortex in places (Fig. 5E).

It is difficult to discern any growth marks in the NMQR 3689a humerus, but three annuli are present in the femur and tibia of this individual (Fig. 5F). Growth marks are present in the rest of the elements as well and consist of annuli of lamellar bone or LAGs (Fig. 5E). Sharpey's fibers were observed in femur NMQR 3699a on the anterior surface, possibly for the insertion of M. adductor femoris (*Ray, 2006*). A region on the posteromedial side of ulna NMQR 3663b consists of collagen fibers and vascular canals that face perpendicularly to the rest of the bone tissues and may represent an area of muscle insertion.

Age Class IV (80%–100%)— Two individuals, both from Permian deposits, were available for study (Table S1). The bones contain small medullary cavities with an extensive spongy region surrounding the cavities (Figs. 6A, 6B). The bone tissues in both individuals consist of fibrolamellar bone, but it becomes parallel-fibered in tibia NMQR 3940b and radius NMQR 3940d. Femur NMQR 1020 contains fibrolamellar bone to the sub-periosteal surface and there is no indication of a decrease in growth rate (Fig. 6C). This individual also exhibits fewer growth marks than humerus NMQR 3663 from Age Class III, with NMQR 3663 being only 3% smaller than NMQR 1020 (Table S1). This difference may be due to intraskeletal or inter-individual variability. NMQR 3940 shows a decreased size in the vascular canals, which become increasingly simple towards the bone periphery (Fig. 6D). Outer circumferential lamellae or OCL (also known as an External Fundamental System) in the form of avascular lamellar bone and or many closely spaced LAGs at the bone periphery, which would indicate that maximum growth had been reached, are absent. An OCL has been observed in the Triassic kannemeyeriiform dicynodonts *Kannemeyeria* and
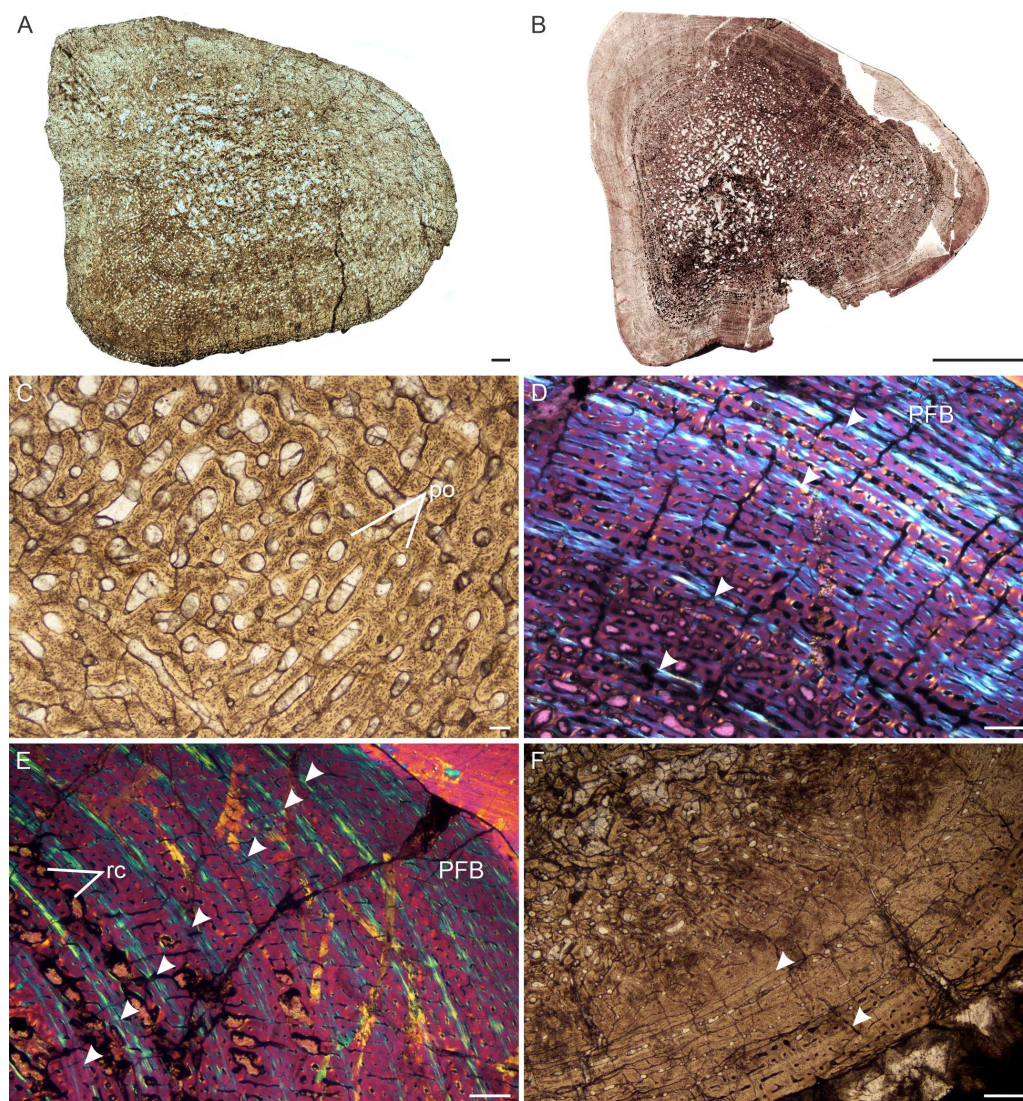
Figure 5 **Transverse sections of the bone histology of *Lystrosaurus maccaigi*, Age Class III.** (A) NMQR 3689a humerus showing an infilled medullary cavity. (B) NMQR 3663a humerus showing the absence of an open medullary cavity. (C) NMQR 3689a humerus showing highly vascularized primary bone tissue. (D) NMQR 3663 humerus showing annuli (arrowheads) and peripheral parallel-fibered bone tissue. (E) NMQR 3663 ulna showing numerous annuli (arrowheads) and peripheral parallel-fibered bone tissue. (F) NMQR 3689c tibia showing two LAGs (arrowheads). Abbreviations: PFB, parallel-fibered bone; PO, primary osteons; RC, resorption cavities. Scale bars equal 500 μm, apart from A, B , which equal 1,000 μm and C, which equals 100 μm.

Placerias (*Botha-Brink & Angielczyk, 2010*; *Green et al., 2010*). Secondary osteons in this individual are more abundant and extend to the sub-periosteal surface in places and have probably resorbed some of the inner growth marks. Up to two generations of secondary osteons were observed (Fig. 6E). Sharpey's fibers were observed in radius NMQR 3940D (Fig. 6F).
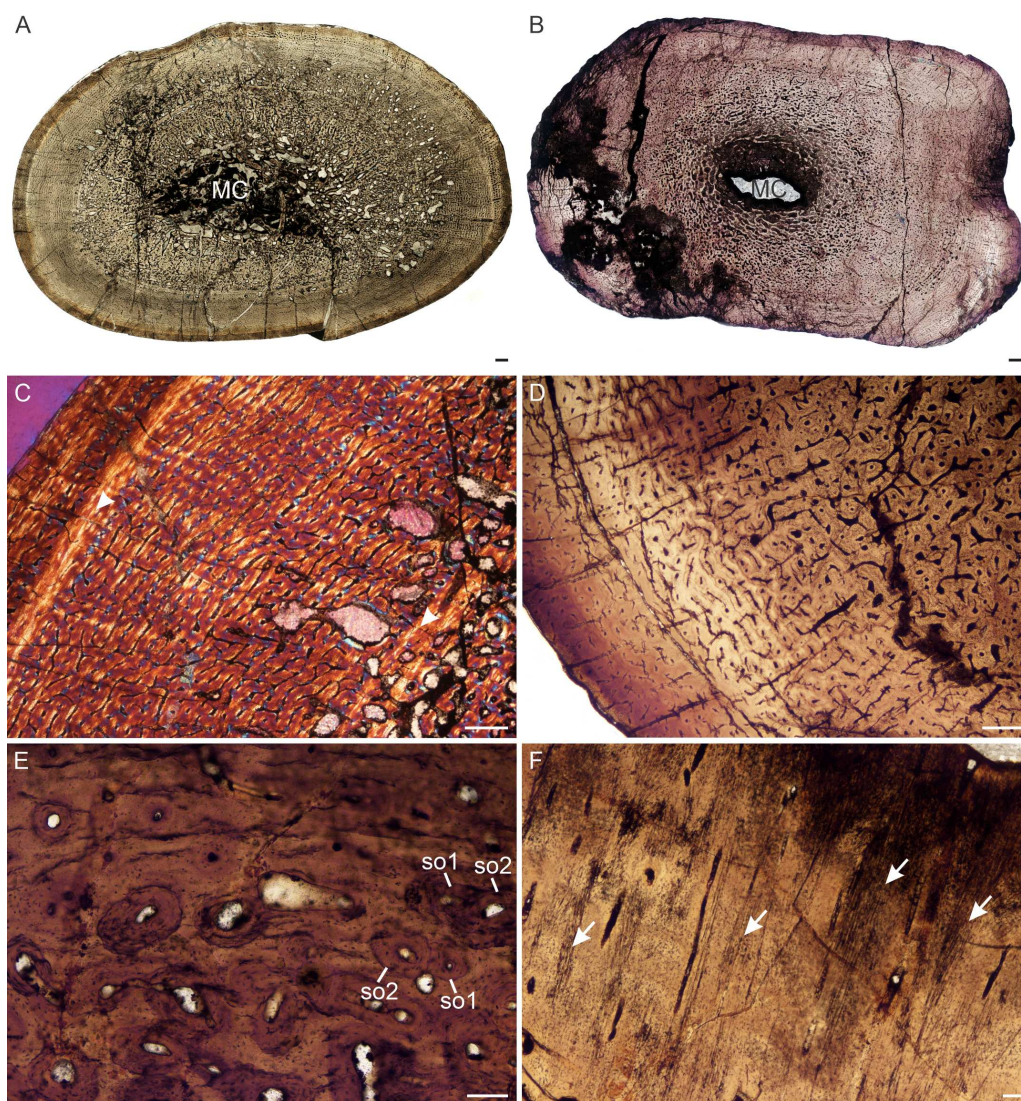
Figure 6 Transverse sections of the bone histology of *Lystrosaurus maccaigi*, **Age Class IV.** (A) NMQR 1020 femur showing an infilled medullary cavity. (B) NMQR 3940b tibia showing a tiny medullary cavity. (C) NMQR 1020 femur in cross-polarized light showing an annulus (arrowhead). (D) NMQR 3940b showing relatively smaller vascular canals towards the sub-periosteal surface. (E) NMQR 3940d radius showing two generations of secondary osteons. (F) NMQR 3940d radius showing Sharpey's fibers (arrows). Abbreviations: MC, medullary cavity; SO, secondary osteon. Scale bars in A and B equal 1,000 μm, C and D equal 500 μm, and E and F equal 100 μm.

L. curvatus

Only specimens belonging to Age Classes I and III were available for study. This is because *L. curvatus* is a rare species with a relatively short stratigraphical range.

Age Class I (<40%)— One individual, NMQR 4001, comprising a humerus, recovered from Triassic deposits, was available for study (Table S1). The medullary cavity is relatively small and open (Fig. 7A). Secondary reconstruction is absent. The bone tissues are similar to
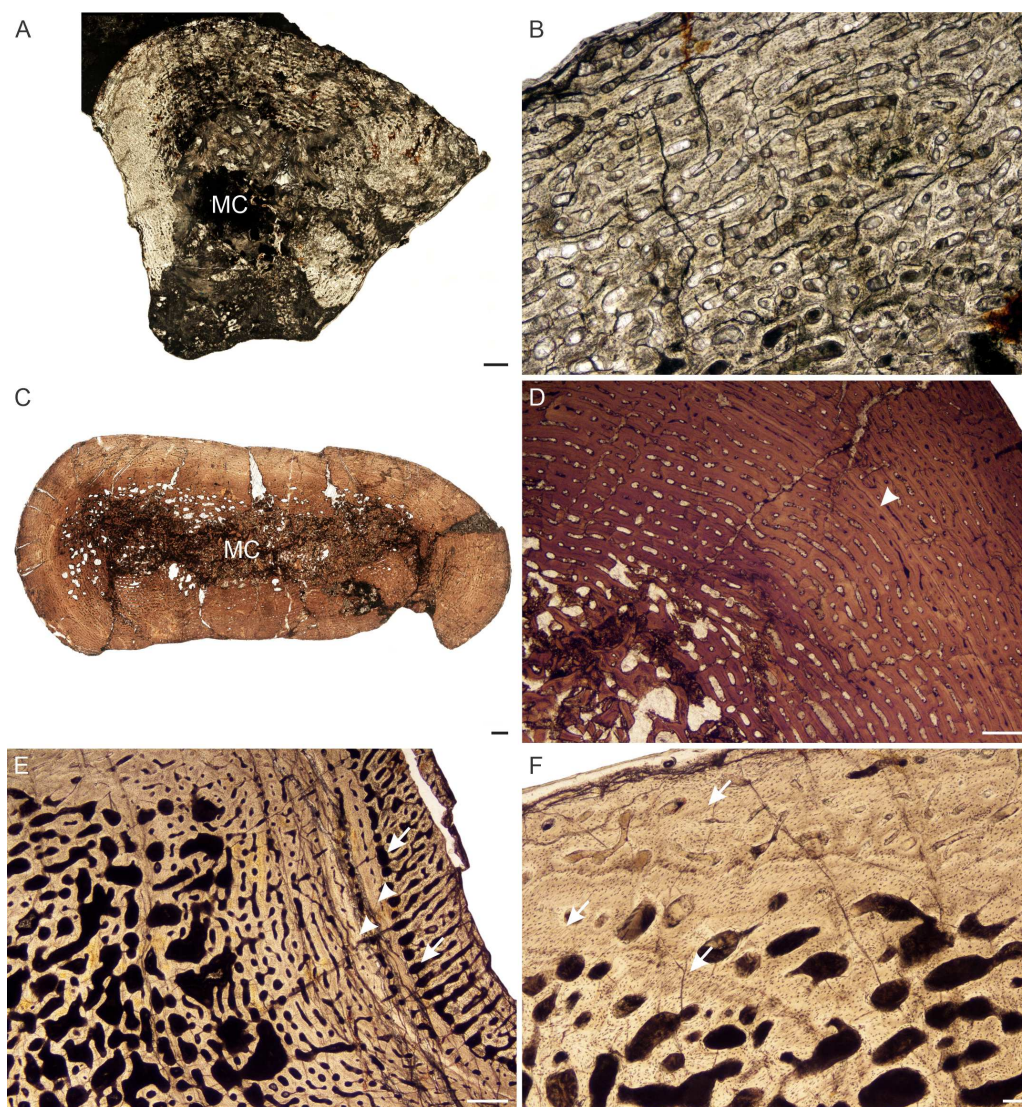
Figure 7 Transverse sections of the bone histology of *Lystrosaurus curvatus*, Age Class I, III. (A)
NMQR 4001 humerus showing a tiny medullary cavity and thick cortex. (B) NMQR 4001 humerus (Age
Class I) showing highly vascularized fibrolamellar bone tissue. (C) NMQR 3922b femur showing bony
trabeculae filling the medullary cavity. (D) NMQR 3922a humerus (Age Class III) showing fibrolamellar
bone in a laminar vascular arrangement interrupted by a LAG (arrowhead). (E) NMQR 3651c ulna (Age
Class III) showing enlarged canals (arrows) following two annuli (arrowheads). (F) NMQR 3651b radius
(Age Class III) showing Sharpey's fibers (arrows). Abbreviations: MC, medullary cavity; PO, primary
osteons. Scale bars in A and B equal 1,000 μm, C and F equal 100 μm, whereas D and E equal 500 μm.

those of *L. maccaigi* for this age class. They consist of highly vascularized fibrolamellar bone
with large (primary osteon diameter 80 μm, Table S1), laminar or longitudinally-oriented
primary vascular canals (Fig. 7B). There is no decrease in vascularization towards the
periphery and growth marks are absent.

Age Class III (60%–79%)— Two individuals comprising a radius, ulna, humeri and
femur, both from Permian deposits, were available for examination (Table S1). The

medullary cavities are infilled with bony trabeculae (Fig. 7C) resulting in a gradual transition zone from cavity to compact cortex (Figs. 2C–2E). The bone tissues continue to contain highly vascularized fibrolamellar bone in a laminar network (Fig. 7D). The size of the vascular canals decreases towards the sub-periosteal surface. Growth marks are present as faint annuli in all the bones. In individual NMQR 3651, which comprises a humerus, radius and ulna, the vascular canals decrease in size towards the annulus and increase in size again after the annulus, showing an increase in growth rate after this growth mark (Fig. 7E). An OCL was not found. Sharpey's fibers were observed in radius NMQR 3651b on the anterolateral side and in ulna NMQR 3651c on the medial side (Fig. 7F).

L. murrayi

Age Class I (<40%)— All *L. murrayi* individuals were recovered from Triassic deposits. Three individuals comprising humeri, radii and ulnae fall into this age class (Table S1). The smallest individual, NMQR 3635, is 22% the maximum known size and represents the smallest individual of the four *Lystrosaurus* species. The medullary cavities of the radius and ulna of this individual are small, but open, with the radius containing one or two loose trabeculae in the cavity. The cortices are relatively thick. The bone tissues are comprised of fibrolamellar bone with large vascular canals arranged longitudinally in circumferential rows around the medullary cavities (Fig. 8A). Secondary reconstruction and growth marks are absent. Sharpey's fibers were observed in the ulna (Fig. 8B). The larger bones in this age class contain similar tissues, but the medullary cavities are increasingly infilled by bony trabeculae.

 Age Class II (40%–59%)— The three individuals (Table S1) comprising humeri, a radius, ulna and femur, contain similar bone tissues to those of Age Class I, i.e., highly vascularized fibrolamellar bone (Fig. 8C). The primary osteons are arranged either in a laminar network or longitudinally in circumferential rows. Resorption cavities and secondary osteons are absent. Growth marks were not observed in any of these bones.

 Age Class III (60%–79%)— Although the bone tissues of these six individuals (comprising all six limb bones) contain similar bone tissues to the earlier age classes (Figs. 8D; 2G, 2H), some of them exhibit growth marks. The humerus of SAM-PK-8991 for example exhibits two growth marks, whereas others in this age class exhibit one or none. The second growth mark in SAM-PK-8991, however, is not clearly defined, but instead is demarcated by a change in the orientation of vascular canals from laminar to radial (Fig. 8E). This observation does not represent a temporary decrease or cessation in bone growth, but possibly a change in season where the bone growth was accelerated (as expressed by the radial canals). However, it should be noted that this condition of radial canals was only observed in the humerus of SAM-PK-8991 and not in the radius and ulna. The canals before the first growth mark in humerus SAM-PK-8991 appear to be primary, but they appear secondarily enlarged after this first growth mark (Fig. 8E). The canals continue in this manner right up to the periphery of the bone. The cortical porosity is also the highest in the *L. murrayi* sample, even compared to ontogenetically younger individuals. These features were not found in any other specimen and may represent some form of pathology. The ulna and radius of this specimen are very poorly preserved with
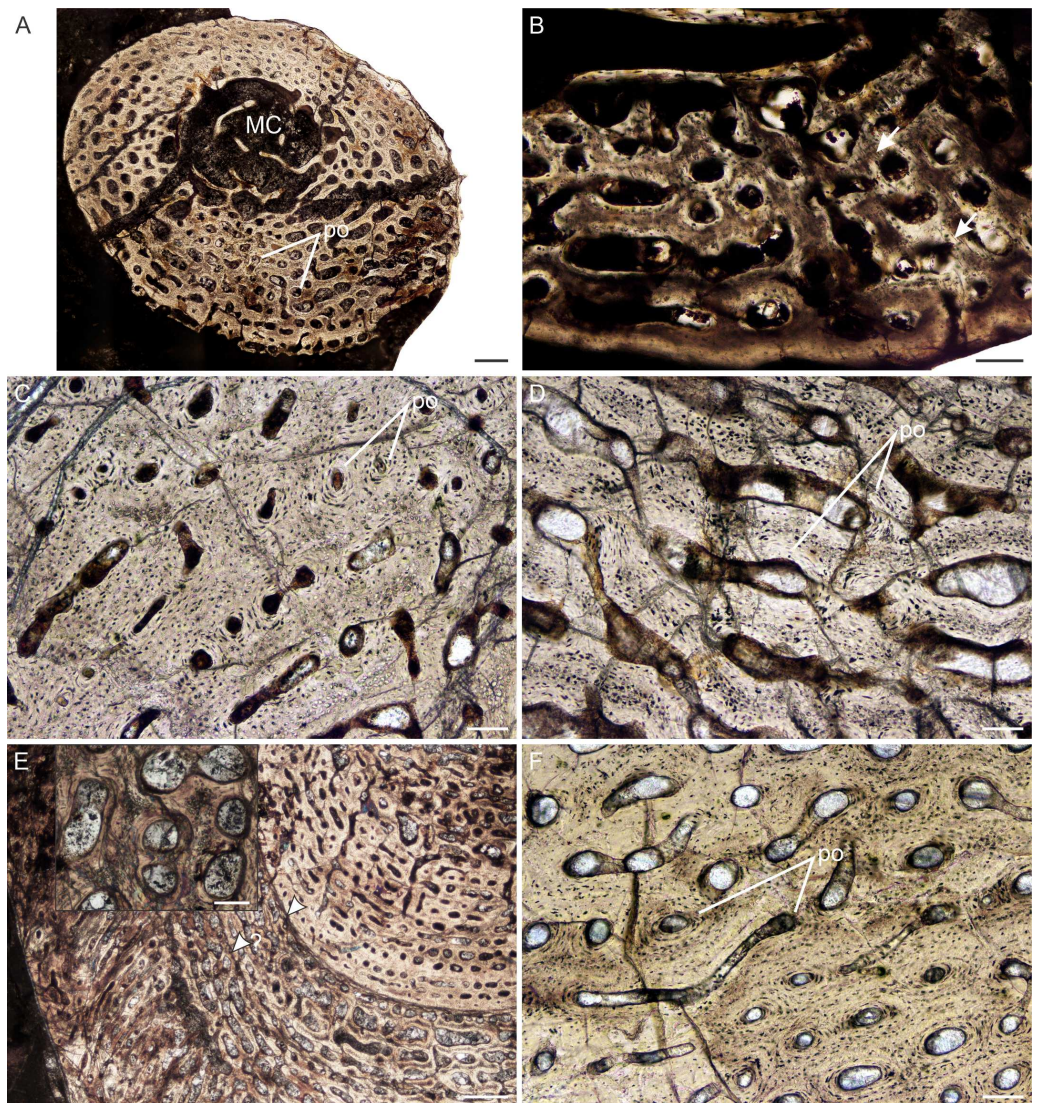
Figure 8 **Transverse sections of the bone histology of *Lystrosaurus murrayi*, Age Class I–IV.** (A) NMQR 3635a radius (Age Class I) showing highly vascularized woven-fibered bone tissue. (B) NMQR 3635b ulna (Age Class I) showing Sharpey's fibers (arrows). (C) NMQR 3927a humerus (Age Class II) showing highly vascularized primary bone tissue. (D) High magnification of humerus BP/1/5070 (Age Class III) showing primary osteons. (E) SAM-PK-8991 (Age Class III) showing a change from laminar to radial vascular canals traversed by two annuli (arrowheads). High magnification insert shows the secondarily enlarged canals. (F) BP/1/3236 humerus (Age Class IV) showing primary bone. Abbreviations: MC, medullary cavity, PO, primary osteons. Scale bars in A and E equal 500 μm, whereas B, C, D and F and insert equal 100 μm.

numerous cracks and thus, it is difficult to determine if the osteons in the mid and outer cortex are primary or secondary.

Age Class IV (80%–100%)— Humerus BP/1/3236 is 100% the maximum known size for *L. murrayi*. A very small clear medullary cavity is surrounded by a large expanse of trabecular bone (Fig. 2F). The compact cortex consists primarily of highly vascularized

fibrolamellar bone tissue (Fig. 8F). The vascular canals are arranged in a laminar network. They decrease in size towards a mid-cortical annulus and then increase in size again after it (Fig. 9A). Only one growth mark was observed. There is a slight decrease in vascular size at the sub-periosteal surface in places, but slower forming bone tissues are absent. Resorption cavities extend into the mid-cortex in some regions. They are identified by their enlarged appearance and uneven borders in the form of Howship's lacunae (Fig. 9B). Isolated secondary osteons were observed, scattered throughout the cortex, but dense Haversian bone is absent (Fig. 9C). An OCL was not observed. There is also no indication of a transformation in the cortex from fibrolamellar bone to slower forming bone tissues such as parallel-fibered or lamellar bone.

L. declivis

There is no Age Class I for this species. The smallest individual is 44% the maximum known size.

Age Class II (40%–59%)— All *L. declivis* specimens were recovered from Triassic deposits. Five individuals comprising all six limb bones were available for study (Table S1). Most of the bones contain very small open medullary cavities, which are then surrounded by a wide region of spongy bone. These bone trabeculae in the peri-medullary region result in a broad transition zone to the compact cortex. The bone tissues are similar to those of *L. murrayi* for this stage, which comprise highly vascularized fibrolamellar bone tissue (Fig. 10A). Some individuals exhibit a single mid-cortical annulus (Fig. 10A), but not all limb bones of an individual present growth marks, nor are their presence linked to size. Resorption cavities are limited to the peri-medullary region, as are small isolated secondary osteons.

Age Class III (60%–79%)— Four individuals comprising humeri, a radius, ulna, femur and ribs fall into this ontogenetic stage (Table S1). Highly vascularized fibrolamellar bone continues to dominate the cortex. Longitudinal sections of humerus NMQR 3181 (77% of the maximum known size) were made and found to preserve an interstitial matrix of disorganized collagen fibers and densely packed randomly distributed globular osteocyte lacunae, confirming the presence of woven-fibered bone even in relatively older individuals belonging to Age Class III (Fig. 10B). A small region of peripheral parallel-fibered bone was observed in rib SAM-PK-K8013a (Fig. 10C), similar to what was described in *Ray, Chinsamy & Bandyopadhyay (2005)*. Annuli were not observed in the smaller bones of this age class apart from a single annulus in rib SAM-PK-11184a. Single annuli were found in the limb bones and ribs of the slightly larger bones (SAM-PK-11184a, SAM-PK-K8013a, NMQR 3181), however. Resorption cavities are present in the peri-medullary region and extend into the mid-cortex in places. Secondary osteons remain isolated and limited to the inner regions of the bones.

Stage Class IV (80%–100%)— A single individual, NMQR 1485, comprising a humerus, radius, ulna and femur represents this ontogenetic stage and is 82% the maximum known size of *L. declivis* (Table S1). The humerus contains a tiny open medullary cavity that is surrounded by an extensive network of bony trabeculae. The other limb bones contain a few loose trabeculae throughout the medullary cavities to some extent (Figs. 2I–2K). The
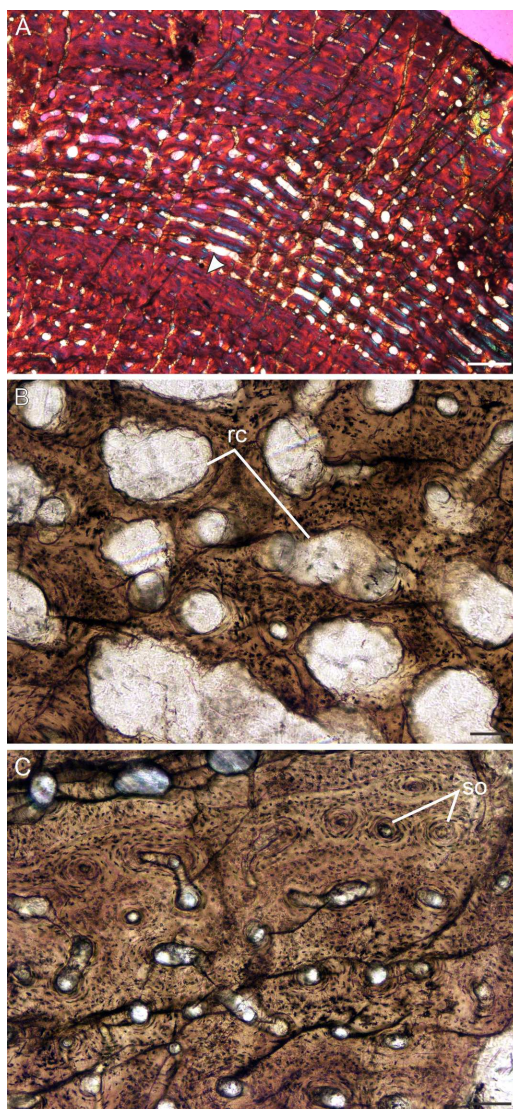
Figure 9 **Transverse sections of the bone histology of *Lystrosaurus murrayi*, Age Class IV.** (A) BP/1/3236 humerus in cross polarized light showing an annulus traversing fibrolamellar bone tissue. (B) BP/1/3236 humerus showing resorption cavities. (C) BP/1/3236 humerus showing secondary osteons. Abbreviations: RC, resorption cavities, SO, secondary osteons. Scale bars in A equal 500 μm, whereas B and C equal 100 μm.

primary bone tissue comprises well vascularized fibrolamellar bone (Fig. 10D), with the humerus and femur having the highest vascularization (Table S1). A single mid-cortical annulus was observed in each limb bone. The ulna may contain two annuli, but the innermost one does not extend around the entire cortex and joins up with the outer one in one area and thus, this inner mark cannot be confirmed as a separate seasonal growth mark. Although there is a slight decrease in the size of some of the vascular canals at the sub-periosteal surface, there is no transition to slower forming tissues and outer circumferential lamellae are absent from the bones indicating that this individual was still
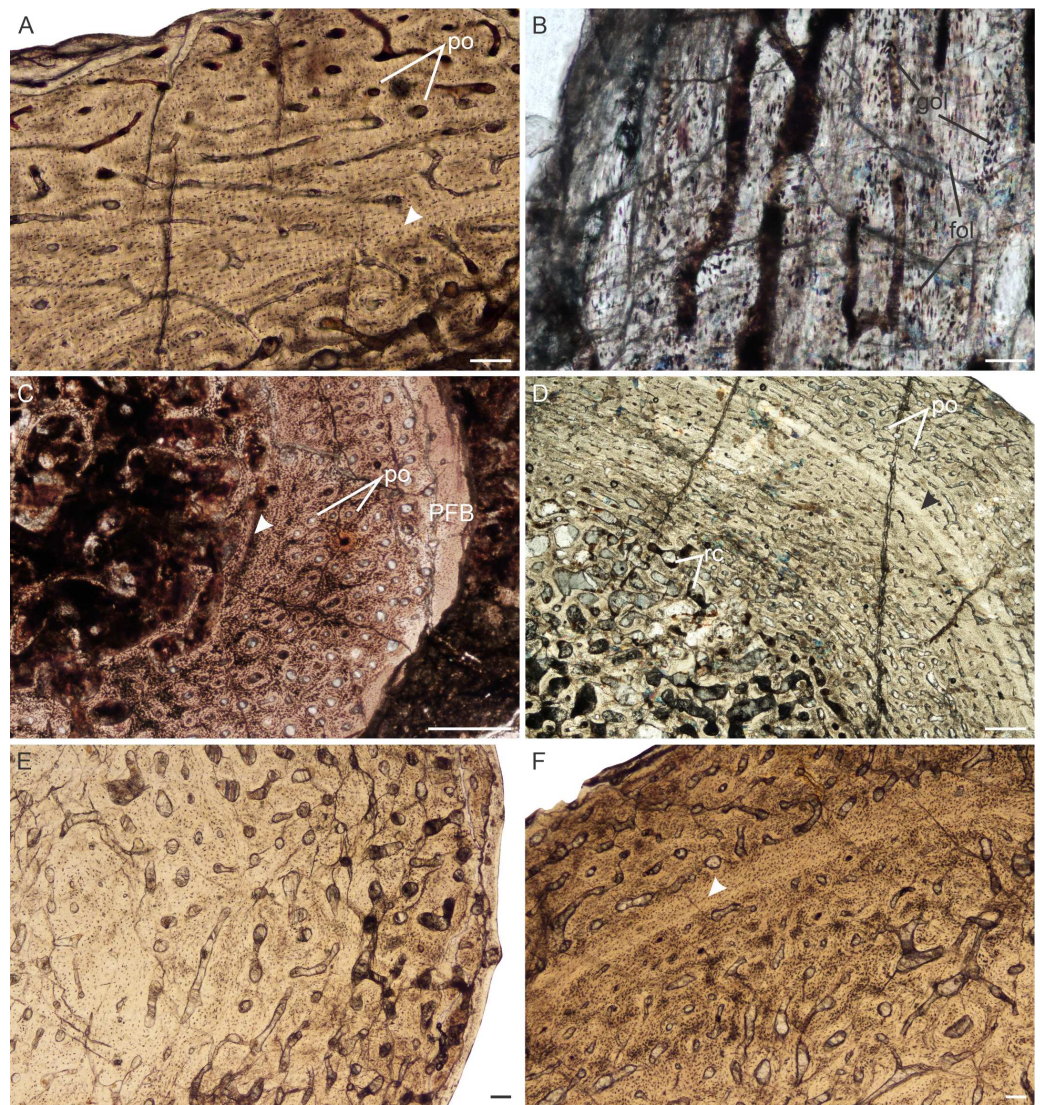
Figure 10 Bone histology of *Lystrosaurus declivis*, Age Class II–IV. (A) Transverse section of NMQR 4039 femur (Age Class II) showing fibrolamellar bone tissue traversed by an annulus. (B) Longitudinal section of NMQR 3181 humerus (Age Class III) showing a mixture of globular and flattened osteocyte lacunae. The large, globular osteocyte lacunae indicate the presence of woven-fibered bone. (C) Transverse section of SAM-PK-K8013a rib (Age Class III) showing primary osteons and peripheral parallel-fibered bone. Arrowhead indicates an annulus. (D) Transverse section of NMQR 1485a humerus (Age Class IV) showing an inner region of resorption cavities and mid- to outer region of fibrolamellar bone. Arrowhead indicates an annulus. (E) Transverse sections of NMQR 1485b radius (Age Class IV) and (F) NMQR 1485c ulna (Age Class IV) showing no decrease in vascularization towards the sub-periosteal surface. Arrow in (F) indicates an annulus. Abbreviations: FOL, flattened osteocyte lacunae; GOL, globular osteocyte lacunae; PFB, parallel-fibered bone tissue; PO, primary osteons; RC, resorption cavities. Scale bars in A and B equal 100 μm, whereas C–F equal 500 μm.

actively growing at the time of death. Resorption cavities extend into the mid-cortex and secondary osteons are found scattered through the bones, but dense Haversian bone is absent. Sharpey's fibers were observed on the anterolateral side of radius NMQR 1485b.

Table 1 Compactness parameters, K and lifestyle readings for the humerus, radius and ulna of the four South African *Lystrosaurus* species, compared to the dicynodontoid *Daptocephalus leoniceps*.

Species	Acc. No.	MD	Min	Max	S	P	Cc	Cp	Cg	K	Lifestyle
Humerus											
L. maccaigi	NMQR 3663a	40	0.3730496	0.999999	0.2038591	0.6227462	0.399	0.913	0.717	0.62	0
L. curvatus	NMQR 3922a	29	0.3879353	0.9234601	0.0748487	0.6072952	0.474	0.931	0.715	0.61	0
L. murrayi	BP/1/3236	30	0.2971604	0.85865	0.118658	0.4562598	0.334	0.825	0.716	0.45	0
L. declivis	NMQR 1485a	28	0.2884796	0.8827366	0.1255311	0.5596468	0.296	0.865	0.669	0.55	0
D. leoniceps	NMQR 3633a	39	0.1910163	0.985676	0.4026052	0.1560593	0.517	0.898	0.798	0.15	0
Radius											
L. curvatus	NMQR 3651b	18	0.2316513	0.999999	0.1180121	0.6902793	–	–	0.61	0.69	0
L. murrayi	NMQR 659b	12	0.1359149	0.9222332	0.0856374	0.387408	–	–	0.783	0.38	0
L. declivis	NMQR 1485c	18	0.0857202	0.9095449	0.0772092	0.5071929	–	–	0.679	0.51	0
Ulna											
L. maccaigi	NMQR 3663b	41	0.3048958	0.999999	0.1806802	0.497793	–	–	0.772	0.49	–
L. curvatus	NMQR 3651c	20	0.4636301	0.9041376	0.1178336	0.6704773	–	–	0.691	0.67	–
L. murrayi	NMQR 659c	19	0.3233334	0.9169428	0.083876	0.4531913	–	–	0.78	0.45	–
L. declivis	NMQR 1485c	23	0.0650608	0.9073332	0.1125244	0.4720466	–	–	0.684	0.47	–

Notes.

Abbreviations: Acc. No, accession number; Cc, compactness at the bone center; Cg, global compactness; Cp, compactness at the bone periphery; Max, maximum compactness; MD, maximum diameter; Min, minimum compactness; K, cortical thickness; P, transition area between the medullary cavity and compact cortex; S, value proportional to the width of the transition zone between the medullary cavity and cortex.

A 0 lifestyle reading for the humerus and radius in all taxa indicates an aquatic lifestyle (*Canoville & Laurin, 2010*; *Laurin, Canoville & Germain, 2011*). There is currently no available model to determine lifestyle using the ulna.

Bone microanatomy

The bone microanatomy of the largest, ontogenetically oldest specimens were examined in order to compare between species (Fig. 2). Thus, only the forelimb bones were studied. The cortical thickness (K in Table 1) ranges from 0.38 to 0.69. The radius and ulna cortices of *L. murrayi* and *L. declivis*, and the ulna of *L. maccaigi* are thick (0.38 to 0.51), whereas the radius and ulna of *L. curvatus* are relatively thinner (radius 0.69; ulna 0.67). The cortical thickness of the *L. murrayi* and *L. declivis* humeri are also relatively thicker compared to *L. maccaigi* and *L. curvatus* (Table 1). However, none of the values compare with the closely related dicynodontoid *Daptocephalus leoniceps*, which has a very thick cortex with a K value of 0.15.

The overall bone compactness (Cg) is similar among the humeri, with *L. declivis* having a slightly lower compactness (Table 1). Both the *L. murrayi* radius and ulna have slightly higher global compactness values than the other *Lystrosaurus* species. The *D. leoniceps* humerus has the highest Cg, but is only slightly higher than the *L. maccaigi*, *L. curvatus* and *L. murrayi* humeri, all of which are similar (0.715–0.717).

The maximum diameter (MD), Min, Max, S, P, Cc, Cp and Cg values were used to predict the lifestyle of the *Lystrosaurus* species and *D. leoniceps* using Bone Profiler for Windows (Table 1). Only the radius and humerus were used to infer lifestyle as there is currently no model available for the ulna. An aquatic lifestyle was predicted for all the *Lystrosaurus* species using either the humerus or radius as well as for the *D. leoniceps* humerus.

DISCUSSION

The predominant bone tissue type in *Lystrosaurus* is fibrolamellar bone, as noted in previous studies (*Ray, Chinsamy & Bandyopadhyay, 2005*; *Botha-Brink & Angielczyk, 2010*; *Botha-Brink et al., 2016*). Highly vascularized fibrolamellar bone with longitudinally-oriented vascular canals characterize the juvenile age class, which becomes increasingly laminar through ontogeny. Incipient fibrolamellar bone (a mixture of parallel-fibered bone and woven-fibered bone, *Klein, 2010*) as described by *Olivier et al. (2017)* in some *Lystrosaurus* elements is only present in older individuals where patches of parallel-fibered bone have appeared between the fibrolamellar bone. Fully developed fibrolamellar bone is present in the juveniles and early subadults.

There is no dominance of secondary osteons or dense Haversian bone in the mid to outer cortex of any of the individuals studied. Erosionally enlarged channels or resorption cavities are limited to the inner cortex and only extend into the mid-cortex in the largest individuals (Age Class IV). *Ray, Chinsamy & Bandyopadhyay (2005)* identified erosionally enlarged channels and profuse secondary osteons in the inner to mid-cortex in their subadult individuals and even during early ontogeny in some cases (e.g., femora 40–50% of their adult size) resulting in a very thin compact cortical region. The size of the primary osteons (measured as the maximum diameter of the entire osteon, Table S1) in the mid-cortical regions of the bones examined in this study is consistent with that of other Permo-Triassic therapsids (see Table S1 of *Botha-Brink et al., 2016* for other therapsid measurements). The largest *L. murrayi* and *L. declivis* individuals do, however, exhibit bands of small channels that either precede or surround a growth mark that are then followed by bands of relatively larger channels. These larger channels appear to be primary with no secondary enlargement (i.e., Howship's lacunae and cement lines are absent, e.g., Figs. 3C, 3E, 3F, 4C, 4E, 5C, 7B, 7D, 9A, 10D). They likely indicate a spurt of rapid growth following a period of slow growth during the unfavorable growing season.

The observation that most of the cortex in the *Lystrosaurus* bones is comprised of primary, rapidly forming fibrolamellar bone, which is highly vascularized indicates rapid growth rates and does not reflect an osteoporotic lifestyle response comprised of secondary bone as proposed by *Ray, Chinsamy & Bandyopadhyay (2005)*. Recent research using isotopes (*Rey et al., 2017*), primary osteon density (or primary osteon area) and phylogenetic eigenvector maps (*Olivier et al., 2017*; *Faure-Brac & Cubo, 2020*), and growth marks in dentine (*Whitney & Sidor, 2020*) have proposed that *Lystrosaurus* was endothermic. *Rey et al. (2017)* and *Faure-Brac & Cubo (2020)* suggest that all Neotherapsida (the clade that includes anomodonts and theriodonts) had an endothermic metabolism. However, it is important to state what kind of endothermy may have been present as there is a whole spectrum of metabolic states from poikilothermic ectothermy in extant reptiles to homeothermic endothermy in extant mammals and birds. It would be interesting to know where dinocephalian therapsids fit into this hypothesis as they are characterized by fibrolamellar bone with relatively large vascular canals and high vascular density (*Botha & Huttenlocker, in press*), but they have yet to be sampled.

Faure-Brac & Cubo (2020) refer to neotherapsid thermometabolism as being "primitively endothermic" and *Whitney & Sidor (2020)* suggest that *Lystrosaurus* was a heterothermic endotherm. It is highly unlikely that *Lystrosaurus* was a homeothermic endotherm as in extant mammals as there are several morphological (and physiological) features that had to be in place prior to the acquisition of homeothermic endothermy. Just two of these features include maxillary turbinates for the conservation of heat and water, and a muscular diaphragm allowing for high ventilation rates, neither of which fossilize. Ossified maxilloturbinate bones (the ridges on which the maxillary turbinate membranes rest) have been found in the Late Triassic-Early Jurassic tritheledontid *Elliotherium* and the mammaliaform *Morganucodon* (*Crompton et al., 2017*). Despite *Laaß et al. (2011)* interpreting structures in the nasal cavity of *Lystrosaurus* as cartilaginous maxilloturbinates (based on neutron tomography), this observation has never been confirmed nor has the feature been found in any other anomodont. If the maxilloturbinates remained cartilaginous during the early part of their evolution they may have been mostly involved in evaporative cooling rather than in water conservation (*Crompton et al., 2017*) and thus, would not have been able to support homeothermic endothermy at this stage. The presence of ribs reaching almost to the pelvic girdle and delicate nature of these bones in *Lystrosaurus* also make it unlikely that a muscular diaphragm was present (Strong, pers. comm., 2012). It is unknown when a mammal-like diaphragm evolved, but the presence of reduced lumbar ribs in the Early Triassic non-mammaliaform cynodont *Thrinaxodon* suggests that there was at least space for such a feature in this clade. Thus, it is likely that *Lystrosaurus* was at most a heterothermic endotherm as suggested by *Whitney & Sidor (2020)*.

The irregular occurrence of growth marks in *L. murrayi* and *L. declivis* is noteworthy and suggests that these species were capable of developmental plasticity. Developmental plasticity is the ability of an organism to change its growth patterns in response to changing environmental conditions. Osteohistological developmental plasticity has been reported in extant amphibians (*Alcobendas & Castanet, 2000*) and birds (*Starck & Chinsamy, 2002*). In extinct vertebrates this feature, in the form of variation in single or double LAGs or number of LAGs and size, has been found in the Permian lissamphibian *Doleserpeton* (*Gee, Haridy & Reisz, 2020*) and the Triassic sauropodomorph dinosaur *Plateosaurus* (*Sander & Klein, 2005*). In this case, *L. murrayi* and *L. declivis* show a variable instance of LAGs at similar body sizes, similar to *Plateosaurus*. *Sander & Klein (2005)* found that growth mark counts were poorly correlated with body size in *Plateosaurus*. They proposed that developmental plasticity in this dinosaur indicated that it was ectothermic as strong developmental plasticity is correlated with low metabolic rates (*Sander & Klein, 2005*). However, there is a variety of research to suggest that dinosaurs were at least partially endothermic (e.g., *Erickson et al., 2009*; *Grady et al., 2014*; *Legendre et al., 2016*; *Rezende et al., 2020*). It is possible that *Lystrosaurus* could have varied its growth as a heterothermic endotherm. This may have been advantageous in the post-extinction Early Triassic environment, which is considered to have undergone extreme temperatures (*Rey et al., 2016*), and would have allowed it to undergo torpor at high latitudes as suggested by *Whitney & Sidor (2020)*.

An overall transition to slower forming bone tissues in the form of parallel-fibered bone is only observed in the very largest *L. maccaigi* specimens. Patches of parallel-fibered bone

can be found in some ontogenetically older individuals of the other species, but this bone tissue type does not dominate the cortex. Outer circumferential lamellae were not found in any specimen in this study, indicating that not even the largest *L. maccaigi* individuals had reached maximum body size. The presence of slower forming tissues in the outer periphery of the largest *L. maccaigi* bones, however, does indicate a decrease in growth rate and that these individuals were at least approaching a growth asymptote.

It has long been noted that *L. murrayi* and *L. declivis* are the smaller of the four South African species (e.g., *Grine et al., 2006*; *Botha & Smith, 2007*; *Botha-Brink et al., 2016*) (Fig. 11; Table S2). As they are purely Triassic species it raises the possibility that *Lystrosaurus* underwent a decrease in body size across the Permo-Triassic boundary similar to the therocephalian *Moschorhinus kitchingi* (*Huttenlocker & Botha-Brink, 2013*). However, it is clear from the results in this study that not even the largest individuals of *L. murrayi* and *L. declivis* recovered to date had begun to reach a growth asymptote as outer circumferential lamellae or an overall transition to slower forming bone tissues are absent from all the study limb bones of these species. The basal skull length (BSL) of the largest *L. murrayi* humerus in this study (BP/1/3236), which is the largest *L. murrayi* specimen known overall, is 213 mm (*Botha-Brink et al., 2016*). It is 55% the size of the largest known *L. maccaigi* specimen (BP/1/4038, BSL 389 mm) and 67% the size of the *L. maccaigi* specimen in this study (NMQR 3663, BSL 319 mm) (Table S2), which exhibits a transition to slower forming bone tissues and thus a decrease in growth rate. Given the absence of such a transition in the *L. murrayi* and *L. declivis* individuals it is likely that all specimens of these species recovered to date represent juvenile or early sub-adult ontogenetic stages. Thus, these two Triassic species were capable of growing to significantly larger sizes and may even have reached similar sizes to *L. maccaigi* and *L. curvatus*. There is thus, no evidence of a Lilliput effect in *Lystrosaurus* during the EPME. The smaller BSL in *L. murrayi* and *L. declivis* are more likely the effect of shorter lifespans where these species were dying at younger ages compared to the Permian species as suggested by *Botha-Brink et al. (2016)*. Thus, although there is evidence of a Lilliput effect in dicynodonts across the PTB with the disappearance of larger taxa (*Angielczyk & Walsh, 2008*) there is no evidence of a dwarfing of *Lystrosaurus* species.

The high abundance of smaller specimens in museum collections is unlikely due to a collection bias as larger specimens are easier to find than smaller specimens. There is a change in taphonomic style from the Permian to Triassic where more articulated skeletons are found in Triassic deposits, but skull material is found equally in both deposits (*Smith & Botha-Brink, 2014*). The burrowing lifestyle of *Lystrosaurus* may also have increased its preservational potential, however, even Permian species of *Lystrosaurus* (e.g., *L. curvatus*, *Botha-Brink, 2017*) were capable of burrowing. Furthermore, a burrowing lifestyle should not bias the preservation of smaller specimens as *Lystrosaurus* is considered to have burrowed throughout its entire lifespan. Thus, even large specimens should preserve as easily as smaller individuals. The abundance of smaller individuals of *Lystrosaurus* in the *Lystrosaurus declivis* Assemblage Zone is likely a real biological phenomenon and not one of taphonomic bias.
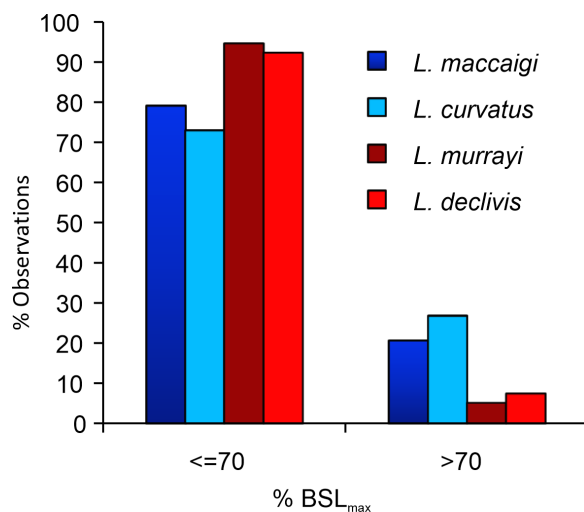
Figure 11 **Percentage of maximum basal skull length (%BSLmax) of the four species of South African** *Lystrosaurus..* There are distinct differences in body size distributions between Permian (blue) and Triassic (red) species (taken from *Botha-Brink et al., 2016*).

A semi-aquatic lifestyle for *Lystrosaurus* was first proposed by *Broom (1902)* and *Broom (1903)* and later supported by several studies (*Watson, 1912*; *Watson, 1913*; *Brink, 1951*; *Camp, 1956*; *Cluver, 1971*; *Hotton, 1986*; *Kemp, 1982*; *Kitching, 1968*) based on various cranial and postcranial morphological features. These studies were later refuted by *King (1991)* and *King & Cluver (1991)* who proposed that the morphological characteristics used to infer an aquatic lifestyle could equally represent a fossorial or burrowing ecology. Later studies (*Smith & Botha, 2005*; *Botha & Smith, 2007*) suggested that an aquatic lifestyle was unlikely given the high abundance and success of *Lystrosaurus* in an increasingly arid environment. However, *Ray, Chinsamy & Bandyopadhyay (2005)* resurrected the aquatic hypothesis based on the microanatomy of *Lystrosaurus* limb bones and ribs where they suggested that the trabecular infilling of the limb bone medullary cavities and high cortical thickness in the ribs was indicative of an amphibious lifestyle.

The most recent study to predict the lifestyle of *Lystrosaurus* is *Canoville & Laurin (2010)* who used a humerus in Bone Profiler and found it to predict an amphibious lifestyle. However, *Kriloff et al. (2008)* also proposed an amphibious lifestyle for *Dicynodon* using the Bone Profiler program, a taxon that is considered to be fully terrestrial based on its morphology. When Bone Profiler was used in this study to predict the lifestyle of *Lystrosaurus* the program also predicted an aquatic lifestyle for all four species. This appears to be based on the trabecular infilling of the medullary cavities. Fully aquatic, pelagic taxa generally exhibit medullary cavities filled with bony trabeculae and broad transition zones that result in a mostly cancellous or very narrow cortex (e.g., the dolphin, *Delphinus delphis*), whereas amphibious shallow water taxa tend to have very thick compact cortices, which help to counteract buoyancy while in the water (e.g., the manatee, *Dugong dugong*) (*Canoville & Laurin, 2010*). The infilled medullary cavities in the limb bones of *Lystrosaurus* would suggest a fully aquatic pelagic lifestyle, but the morphology of this genus

(and dicynodonts as a clade) is inconsistent with a pelagic ecology and rather suggests a fully terrestrial mode of life. Given that the genus *Lystrosaurus* was a relatively large taxon (and that all four species may have grown equally large), it is possible that the trabecular infilling increased the overall strength of the bones and would have been a biomechanical advantage in a fossorial animal. Trabecular infilling of limb bone medullary cavities has been observed in several other dicynodont taxa such as *Rhachiocephalus*, *Aulacephalodon*, *Daptocephalus* and *Kannemeyeria* (*Botha-Brink & Angielczyk, 2010*; *Ray, Botha-Brink & Chinsamy, 2012*) and may have thickened the bones and acted as buttresses against the weight of these animals.

Given these results, it is thus worth cautioning against using Bone Profiler as the only tool to infer lifestyle for anomodonts. Other studies have found similar issues with using bone microanatomy to infer lifestyle for the pelycosaur *Ophiacodon* (see discussions in *Germain & Laurin, 2005*; *Felice & Angielczyk, 2014*; *Laurin & De Buffrenil, 2016*; *Huttenlocker & Shelton, 2020*). The biomechanics of therapsids have no modern analogues with respect to stance and locomotory gait (e.g., the sprawling forelimbs and erect hind limbs), and thus, other factors may have played a role in shaping the bone microanatomy in anomodont therapsids.

CONCLUSION

The highly vascularized fibrolamellar bone present in all four species of South African *Lystrosaurus* indicates that the genus grew rapidly during early to mid-ontogeny, similar to many other Permo-Triassic dicynodonts. There is no notable difference in bone tissues between the four species, except that growth marks are rare and inconsistently present in *L. murrayi* and *L. declivis* specimens of similar body size. This suggests that developmental plasticity may have been present in these taxa and may have been advantageous in the unpredictable post-extinction Early Triassic environment. A transition to slower forming parallel-fibered bone can be seen in older individuals of Permian *L. maccaigi*. The absence of slower forming bone tissues or outer circumferential lamellae in *L. curvatus*, *L. murrayi* and *L. declivis* indicates that even the largest specimens were not close to a growth asymptote. Thus, there is no evidence of a Lilliput effect in South African *Lystrosaurus* in the form of dwarfing of the Triassic species, contrary to another EPME survivor, the therocephalian *Moschorhinus kitchingi*.

Despite some previous studies suggesting that *Lystrosaurus* was aquatic, this study supports a terrestrial mode of life. The trabecular infilling of the medullary cavities is similar to that found in some other large dicynodonts with no morphological aquatic characteristics. Medullary cavity infilling may have been a biomechanical mechanism for supporting the weight of these animals.

Funding

This work was supported by the National Research Foundation (UID 117704, 104688), the Palaeontological Scientific Trust (PAST), and the DST-NRF Centre of Excellence in Palaeosciences (CoE-Pal). The funders had no role in study design, data collection and analysis, decision to publish, or preparation of the manuscript.

Grant Disclosures

The following grant information was disclosed by the author:
National Research Foundation: UID 117704, 104688.
The Palaeontological Scientific Trust (PAST).
DST-NRF Centre of Excellence in Palaeosciences (CoE-Pal).

Competing Interests

The authors declare there are no competing interests.

Author Contributions

- Jennifer Botha conceived and designed the experiments, performed the experiments, analyzed the data, prepared figures and/or tables, authored or reviewed drafts of the paper, and approved the final draft.

Data Availability

The raw measurements are available in the Supplemental File.

Supplemental Information

Supplemental information for this article can be found online at http://dx.doi.org/10.7717/peerj.10408#supplemental-information.

REFERENCES

Alcobendas M, Castanet J. 2000. Bone growth plasticity among populations of *Salamandra salamandra*: interactions between internal and external factors. *Herpetologica* **56(1)**:14–26.

Algeo TJ, Chen ZQ, Fraiser ML, Twitchett RJ. 2011. Terrestrial–marine teleconnections in the collapse and rebuilding of Early Triassic marine ecosystems. *Palaeogeography, Palaeoclimatology, Palaeoecology* **308**:1–11 DOI 10.1016/j.palaeo.2011.01.011.

Amprino R. 1947. La structure du tissue osseux envisage comme expression de differences dans la vitesse de l'accroissement. *Archives de Biologie* **58**:315–330.

Angielczyk KD, Walsh ML. 2008. Patterns in the evolution of nares size and secondary palate length in anomodont therapsids (Synapsida): implications for hypoxia as a cause of end-Permian tetrapod extinctions. *Journal of Paleontology* **82(3)**:528–542 DOI 10.1666/07-051.1.

Benton MJ, Newell AJ. 2014. Impacts of global warming on Permo-Triassic terrestrial ecosystems. *Gondwana Research* **25(4)**:1308–1337.

Benton MJ, Twitchett RJ. 2003. How to kill (almost) all life: the end-Permian extinction event. *Trends in Ecology and Evolution* **18(7)**:358–365 DOI 10.1016/S0169-5347(03)00093-4.

Botha J, Huttenlocker AK. Non-mammalian synapsids. In: De Buffrénil V, Zylberberg L, Padian K, de Ricqlés A, eds. *Comparative skeletal histology and paleohistology.* Boca Raton: CRC Press, Taylor and Francis, in press.

Botha J, Huttenlocker AK, Smith RMH, Prevec R, Viglietti P, Modesto SP. 2020. New geochemical and palaeontological data from the Permian-Triassic boundary in the South African Karoo Basin test the synchronicity of terrestrial and marine extinctions. *Palaeogeography, Palaeoclimatology, Palaeoecology* DOI 10.1016/j.palaeo.2019.109467.

Botha J, Smith R. 2006. Rapid vertebrate recuperation in the Karoo Basin of South Africa following the end-Permian extinction. *Journal of African Earth Sciences* **45(4–5)**:502–514 DOI 10.1016/j.jafrearsci.2006.04.006.

Botha J, Smith R. 2007. *Lystrosaurus* species composition across the Permo-Triassic boundary of South Africa. *Lethaia* **40(2)**:125–137 DOI 10.1111/j.1502-3931.2007.00011.x.

Botha J, Smith RMH. 2020. Biostratigraphy of the *Lystrosaurus declivis* Assemblage Zone *in* R. M. H. Smith (ed.), Karoo biostratigraphy. Special Issue. *South African Journal of Geology* **123(2)**:207–216 DOI 10.25131/sajg.123.0015.

Botha-Brink J. 2017. Burrowing in *Lystrosaurus*: preadaptation to a postextinction environment? *Journal of Vertebrate Paleontology* **37(5)**:e1365080 DOI 10.1080/02724634.2017.1365080.

Botha-Brink J, Angielczyk KD. 2010. Do extraordinarily high growth rates in Permo-Triassic dicynodonts (Therapsida, Anomodontia) explain their success before and after the end-Permian extinction? *Zoological Journal of the Linnean Society* **160**:341–365 DOI 10.1111/j.1096-3642.2009.00601.x.

Botha-Brink J, Huttenlocker A, Angielczyk KD, Codron D, Ruta M. 2016. Breeding young as a survival strategy during Earth's greatest mass extinction. *Scientific Reports* **6**:24053 DOI 10.1038/srep24053.

Botha-Brink J, Huttenlocker AK, Modesto SP. 2014. Vertebrate Paleontology of Nooitgedacht 68: a *Lystrosaurus maccaigi*-rich Permo-Triassic boundary locality in South Africa. In: Kammerer CF, Angielczyk KD, Fröbisch J, eds. *The early evolutionary history of the Synapsida.* Dordrecht: Springer, 289–304.

Brink AS. 1951. On the genus *Lystrosaurus* Cope. *Transactions of the Royal Society of South Africa* **33**:107–120 DOI 10.1080/00359195109519880.

Brook BW, Bowman DMJS. 2002. Explaining the Pleistocene megafaunal extinctions: models, chronologies, and assumptions. *Proceedings of the National Academy of Sciences* **99**:14624–14627 DOI 10.1073/pnas.232126899.

Broom R. 1902. On the leg and toe bones of *Ptychosiagum. Transactions of the South African Philosophical Society* **11**:233–235.

Broom R. 1903. On the structure of the shoulder girdle in *Lystrosaurus. Annals of the South African Museum* **4**:139–141.

Buffetaut E. 2006. Continental vertebrate extinctions at the Triassic–Jurassic and Cretaceous–Tertiary boundaries: a comparison. *Biological processes associated with impact events.* Berlin: Springer.

Burgess SD, Bowring SA, Shen S-Z. 2014. High-precision timeline for Earth's most severe extinction. *Proceedings of the National Academy of Science* **111**:3316–3321 DOI 10.1073/pnas.1317692111.

Camp CL. 1956. Triassic dicynodont reptiles. Part II. In: Triassic dicynodonts compared. *Memoirs of the University of California* **13**:305–348.

Canoville A, Laurin M. 2010. Evolution of humeral microanatomy and lifestyle in amniotes, and some comments on palaeobiological inferences. *Biological Journal of the Linnean Society* **100**:384–406 DOI 10.1111/j.1095-8312.2010.01431.x.

Chen Z-Q, Benton MJ. 2012. The timing and pattern of biotic recovery following the end-Permian mass extinction. *Nature Geoscience* **5**:375–383 DOI 10.1038/ngeo1475.

Chinsamy A. 1990. Physiological implications of the bone histology of *Syntarsus rhodesiensis* (Saurischia: Theropoda). *Palaeontologia Africana* **27**:77–82.

Chinsamy A. 1991. The osteohistology of femoral growth within a clade: a comparison of the crocodile *Crocodylus,* the dinosaurs *Massospondylus* and *Syntarsus,* and the birds *Struthio* and *Sagittarius.* PhD dissertation, University of Witwatersrand, Johannesburg, 200pp.

Chinsamy A. 1995. Ontogenetic changes in the bone histology of the Late Jurassic ornithopod *Dryosaurus lettowvorbecki. Journal of Vertebrate Paleontology* **15(1)**:96–104 DOI 10.1080/02724634.1995.10011209.

Chinsamy A, Rubidge BS. 1993. Dicynodont (Therapsida) bone histology: phylogenetic and physiological implications. *Palaeontologia Africana* **30**:97–102.

Cluver MA. 1971. The cranial morphology of the dicynodont genus *Lystrosaurus. Annals of the South African Museum* **56**:155–274.

Cosgriff JW, Hammer WR, Ryan WJ. 1982. The Pangaean reptile, *Lystrosaurus maccaigi,* in the Lower Triassic of Antarctica. *Journal of Paleontology* **56(2)**:371–385.

Crompton AW, Owerkowicz T, Bhullar B-AS, Musinsky C. 2017. Structure of the nasal region of non-mammalian cynodonts and mammaliaforms: speculations on the evolution of mammalian endothermy. *Journal of Vertebrate Paleontology* DOI 10.1080/02724634.2017.1269116.

Currey JD, Alexander MR. 1985. The thickness of the walls of tubular bones. *Journal of Zoology, London* **206**:453–468.

Ecker M, Botha-Brink J, Lee-Thorp JA, Horwitz LK. 2015. Ostrich eggshell as a source of palaeoenvironmental information in the arid interior of South Africa. In: Runge J, ed. *Changing climates, ecosystems and environments within arid southern Africa and adjoining regions: Palaeoecology of Africa 33.* Kentucky: CRC Press, 95–111.

Erickson GM, Makovicky PJ, Inouye BD, Chang-Fu Z, Ke-Qin G. 2009. A life table for *Psittacosaurus lujiatunensis*: initial insights into ornithischian population biology. *Anatomical Record* **292**:1514–1521 DOI 10.1002/ar.20992.

Erwin DH. 2006. *Extinction! How life nearly ended 250 million years ago*. Princeton: Princeton University Press.

Erwin DH, Bowring SA, Yugan J. 2002. End-Permian mass extinctions: a review. *Geological Society of America Special Papers* **356**:363–383.

Faure-Brac MG, Cubo J. 2020. Were the synapsids primitively endotherms? A palaeohistological approach using phylogenetic eigenvector maps. *Philosophical Transactions of the Royal Society B* **375**:201901 DOI 10.1098/rstb.2019.0138.

Felice RN, Angielczyk KD. 2014. Was *Ophiacodon* (Synapsida, Eupelycosauria) a swimmer? A test using vertebral dimensions. In: Kammerer CF, Angielczyk KD, Fröbisch J, eds. *Early evolutionary history of the Synapsida*. Netherlands: Springer, 25–51.

Francillon-Vieillot H, De Buffrénil V, Castanet J, Geraudie J, Meunier FJ, Sire JY, Zylberberg L, De Ricqlès A. 1990. Microstructure and mineralization of vertebrate skeletal tissues. In: Carter JG, ed. *Skeletal biomineralization: patterns, processes and evolutionary trends*. 47. New York: Van Nestrand Reinhold, 1–548.

Gastaldo RA, Kamo SL, Neveling J, Geissman W, Looy CV, Martini AM. 2020. The base of the *Lystrosaurus* Assemblage Zone, Karoo Basin, predates the end-Permian marine extinction. *Nature Communications* **11**:1428 DOI 10.1038/s41467-020-15243-7.

Gee BM, Haridy Y, Reisz RR. 2020. Histological skeletochronology indicates developmental plasticity in the early Permian stem lissamphibian *Doleserpeton annectens*. *Ecology and Evolution* **10**:2153–2169 DOI 10.1002/ece3.6054.

Germain D, Laurin M. 2005. Microanatomy of the radius and lifestyle in amniotes (Vertebrata, Tetrapoda). *Zoologica Scripta* **34**:335–350 DOI 10.1111/j.1463-6409.2005.00198.x.

Girondot M, Laurin M. 2003. Bone Profiler: a tool to quantify, model, and statistically compare bone-section compactness profiles. *Journal of Vertebrate Paleontology* **23**:458–461 DOI 10.1671/0272-4634(2003)023[0458:BPATTQ]2.0.CO;2.

Gower DJ, Butler RJ, Sennikov AG, Hancox J, Botha-Brink J. 2014. A new species of *Garjainia ochev*, 1958 (Diapsida: Archosauriformes: Erythrosuchidae) from the Early Triassic of South Africa. *PLOS ONE* **11**:e111154 DOI 10.1371/journal.pone.0111154.

Grady JM, Enquist BJ, Dettweiler-Robinson E, Wright NA, Smith FA. 2014. Evidence for mesothermy in dinosaurs. *Science* **344**:1268–1272 DOI 10.1126/science.1253143.

Green JL, Schweitzer MH, Lamm E-T. 2010. Limb bone histology and growth in Placerias hesternus (Therapsida: Anomodontia) from the Upper Triassic of North America. *Palaeontology* **53**:347–364.

Grine FE, Forster CA, Cluver MA, Georgi JA. 2006. Cranial variability, ontogeny and taxonomy of *Lystrosaurus* from the Karoo Basin of South Africa: Amniote Paleobiology. In: Carrano M, Blob RW, Gaudin TJ, Wible JR, eds. *Perspectives on the evolution of mammals, birds, and reptiles*. Chicago: University of Chicago Press 432–503.

Harries PJ, Knorr PO. 2009. What does the 'Lilliput Effect'mean? *Palaeogeography, Palaeoclimatology, Palaeoecology* **284**:4–10.

Horner JR, De Ricqlès A, Padian K. 1999. Variation in dinosaur skeletochronology indicators: implications for age assessment and physiology. *Paleobiology* **25**:295–304 DOI 10.1017/S0094837300021308.

Hotinski RM, Bice KL, Kump LR, Najjar RG, Arthur MA. 2001. Ocean stagnation and end-Permian anoxia. *Bulletin Geological Society of America* **29**:7–10.

Hotton III N. 1986. Dicynodonts and their role as primary consumers. In: Hotton III N, MacLean PD, Roth JJ, Roth EC, eds. *Ecology and biology of mammal-like reptiles.* Washington: Smithsonian Institution Press, 71–82.

Huttenlocker AK, Botha-Brink J. 2013. Body size and growth patterns in the therocephalian *Moschorhinus kitchingi* (Therapsida: Eutheriodontia) before and after the end-Permian extinction in South Africa. *Paleobiology* **39(2)**:253–277 DOI 10.1666/12020.

Huttenlocker AK, Botha-Brink J. 2014. Bone microstructure and the evolution of growth patterns in Permo-Triassic therocephalians (Amniota, Therapsida) of South Africa. *PeerJ* **2**:e325 DOI 10.7717/peerj.325.

Huttenlocker AK, Shelton CD. 2020. Bone histology of varanopids (Synapsida) from Richards Spur, Oklahoma, sheds light on growth patterns and lifestyle in early terrestrial colonizers. *Philosophical Transactions of the Royal Society B* **375(1793)**:20190142 DOI 10.1098/rstb.2019.0142.

Hutton JM. 1986. Age determination of living Nile crocodiles from the cortical stratification of bone. *Copeia* **2**:332–341.

Irmis RB, Whiteside JH. 2012. Delayed recovery of non-marine tetrapods after the end-Permian mass extinction tracks global carbon cycle. *Proceedings of the Royal Society B* **279**:1310–1318 DOI 10.1098/rspb.2011.1895.

Isozaki Y. 1997. Permo-Triassic boundary superanoxia and stratified superocean: records from lost deep sea. *Science* **276**:235–238 DOI 10.1126/science.276.5310.235.

Jasinoski SC, Chinsamy-Turan A. 2012. Biological inferences of the cranial microstructure of the dicynodonts *Oudenodon* and *Lystrosaurus*. In: Chinsamy-Turan A, ed. *Forerunners of mammals: radiation, histology, biology.* Bloomington: Indiana University Press, 149–178.

Jeffery CH. 2001. Heart urchins at the Cretaceous/Tertiary boundary: a tale of two clades. *Paleobiology* **27(1)**:140–158 DOI 10.1666/0094-8373(2001)027<0140:HUATCT>2.0.CO;2.

Kaljo D. 1996. Diachronous recovery patterns in Early Silurian corals, graptolites and acritarchs. In: Hart MB, ed. *Biotic recovery from mass extinction events.* Vol.102. London: Geological Society Special Publication, 127–133.

Kemp TS. 1982. *Mammal-like reptiles and the origin of mammals.* London: Academic Press, 363 p.

King GM. 1991. The aquatic *Lystrosaurus*: a palaeontological myth. *Historical Biology* **4**:285–322.

King GM, Cluver MA. 1991. The aquatic *Lystrosaurus*: an alternative lifestyle. *Historical Biology* **4**:323–342.

Kitching JW. 1968. On the *Lystrosaurus* Zone and its fauna with special reference to some immature Lystrosauridae. *Palaeontologia Africana* **11**:61–76.

Klein N. 2010. Long bone histology of sauropterygia from the lower Muschelkalk of the Germanic basin provides unexpected implications for phylogeny. *PLOS ONE* **5**:e11613 DOI 10.1371/journal.pone.0011613.

Knoll AH, Bambach RK, Canfield DE, Grotzinger JF. 1996. Comparative Earth history and the Late Permian mass extinction. *Science* **273**:452–457 DOI 10.1126/science.273.5274.452.

Knoll AH, Bambach RK, Payne JL, Pruss S, Fischer WW. 2007. Paleophysiology and end-Permian mass extinction. *Earth and Planetary Science Letters* **256**:295–313 DOI 10.1016/j.epsl.2007.02.018.

Kriloff A, Germain D, Canoville A, Vincent P, Sache M, Laurin M. 2008. Evolution of bone microanatomy of the tetrapod tibia and its use in palaeobiological inference. *Journal of Evolutionary Biology* **21**:807–826 DOI 10.1111/j.1420-9101.2008.01512.x.

Krull ES, Retallack GJ, Campbell HJ, Lyon GL. 2000. $^{13}C_{org}$ chemostratigraphy of the Permian-Triassic boundary in the Maitai Group, New Zealand: evidence for high-latitudinal methane release. *New Zealand Journal of Geology and Geophysics* **43(1)**:21–32 DOI 10.1080/00288306.2000.9514868.

Kump LR, Pavlov A, Arthur MA. 2005. Massive release of hydrogen sulfide to the surface ocean and atmosphere during intervals of oceanic anoxia. *Geology* **33(5)**:397–400 DOI 10.1130/G21295.1.

Laaß M, Hampe O, Schudack M, Hoff C, Kardjilov N, Hilger A. 2011. New insights into the respiration and metabolic physiology of *Lystrosaurus*. *Acta Zoologica* **92**:363–371 DOI 10.1111/j.1463-6395.2010.00467.x.

Laurin M, De Buffrénil V. 2016. Microstructural features of the femur in early ophia-codontids: a reappraisal of ancestral habitat use and lifestyle of amniotes. *Comptes Rendus Palevol* **15**:115–127 DOI 10.1016/j.crpv.2015.01.001.

Laurin M, Canoville A, Germain D. 2011. Bone microanatomy and lifestyle: a descriptive approach. *Comptes Rendus Palevol* **10**:381–402 DOI 10.1016/j.crpv.2011.02.003.

Laurin M, Girondot M, Loth M-M. 2004. The evolution of long bone microanatomy and lifestyle in lissamphibians. *Paleobiology* **30**:589–613 DOI 10.1666/0094-8373(2004)030<0589:TEOLBM>2.0.CO;2.

Legendre LJ, Guénard G, Botha-Brink J, Cubo J. 2016. Palaeohistological evidence for ancestral endothermy in archosaurs. *Systematic Biology* **65**:989–996 DOI 10.1093/sysbio/syw033.

Luo G, Lai X, Shi GR, Jiang H, Yin H, Xie S, Tong J, Zhang K, He W, Wignall PB. 2008. Size variation of conodont elements of the *Hindeodus-Isarcicella* clade during the Permian-Triassic transition in South China and its implication for mass extinction. *Palaeogeography, Palaeoclimatology, Palaeoecology* **264**:176–187 DOI 10.1016/j.palaeo.2008.04.015.

MacDougall MJ, Brocklehurst N, Fröbisch J. 2019. Species richness and disparity of parareptiles across the end-Permian mass extinction. *Proceedings of the Royal Society B* **286(1899)**:20182572 DOI 10.1098/rspb.2018.2572.

MacLeod GK, Quinton PC, Bassett DJ. 2017. Warming and increased aridity during the earliest Triassic in the Karoo Basin, South Africa. *Geology* **45(6)**:483–486.

Margerie E, Cubo J de, Castanet J. 2002. Bone typology and growth rate: testing and quantifying 'Amprino's rule' in the mallard (*Anas platyrhynchos*). *Les Comptes Rendus de l' Academie des sciences, Série Biologies* **325**:221–230 DOI 10.1016/S1631-0691(02)01429-4.

Margerie E de, Robin J-P, Verrier D, Cubo J, Groscolas R, Castanet J. 2004. Assessing a relationship between bone microstructure and growth rate: a fluorescent labelling study in the king penguin chick (*Aptenodytes patagonicus*). *The Journal of Experimental Biology* **207**:869–879 DOI 10.1242/jeb.00841.

Metcalfe B, Twitchett RJ, Price-Lloyd N. 2011. Changes in size and growth rate of 'Lilliput'animals in the earliest Triassic. *Palaeogeography, Palaeoclimatology, Palaeoecology* **308**:171–180 DOI 10.1016/j.palaeo.2010.09.011.

Nesbitt SJ, Barrett PM, Werning S, Sidor CA, Charig AJ. 2013. The oldest dinosaur? A Middle Triassic dinosauriform from Tanzania. *Biology Letters* **9(1)**:20120949 DOI 10.1098/rsbl.2012.0949.

Olivier C, Houssaye A, Jalil N-E, Cubo J. 2017. First palaeohistological inference of resting metabolic rate in an extinct synapsid, *Moghreberia nmachouensis* (Therapsida: Anomodontia). *Biological Journal of the Linnean Society* **121**:409–419 DOI 10.1093/biolinnean/blw044.

Payne JL, Clapham ME. 2012. End-Permian mass extinction in the oceans: an ancient analog for the twenty-first century? *Annual Reviews in Earth and Planetary Science* **40**:89–111 DOI 10.1146/annurev-earth-042711-105329.

Ray S. 2006. Functional and evolutionary aspects of the postcranial anatomy of dicynodonts (Synapsida, Therapsida). *Palaeontology* **49(6)**:1263–1286 DOI 10.1111/j.1475-4983.2006.00597.x.

Ray S, Bandyopadhyay S, Bhawal D. 2009. Growth patterns as deduced from bone microstructure of some selected neotherapsids with special emphasis on dicynodonts: phylogenetic implications. *Palaeoworld* **18**:53–66 DOI 10.1016/j.palwor.2008.09.001.

Ray S, Botha-Brink J, Chinsamy A. 2012. Dicynodont growth dynamics and lifestyle adaptations. In: Chinsamy-Turan A, ed. *The forerunners of mammals: radiation, histology and biology.* Bloomington: Indiana University Press, 121–146.

Ray S, Chinsamy A, Bandyopadhyay S. 2005. *Lystrosaurus murrayi* (Therapsida, Dicynodontia): bone histology, growth and lifestyle adaptations. *Palaeontology* **48**:1169–1185 DOI 10.1111/j.1475-4983.2005.00513.x.

Renaud S, Girard C. 1999. Strategies of survival during extreme environmental perturbations: evolution of conodonts in response to the Kellwasser crisis (Upper Devonian). *Palaeogeography, Palaeoclimatology, Palaeoecology* **146**:19–32 DOI 10.1016/S0031-0182(98)00138-2.

Retallack GJ. 2013. Permian and Triassic greenhouse crises. *Gondwana Research* **24**:901–903 DOI 10.1016/j.gr.2012.03.003.

Rey K, Amiot R, Fourel F, Abdala F, Fluteau F, Jalil N-E, Liu J, Rubidge BS, Smith RMH, Steyer JS, Viglietti PA, Wang X, Lécuyer C. 2017. Oxygen isotopes suggest elevated thermometabolism within multiple Permo-Triassic therapsid clades. *eLife* **6**:e28589 DOI 10.7554/eLife.28589.

Rey K, Amiot R, Fourel F, Rigaudier T, Abdala F, Day MO, Fernandez V, Fluteau F, France-Lanord C, Rubidge BS, Smith RMH, Viglietti PA, Zipfel B, Lécuyer C. 2016. Global climate perturbations during the Permo-Triassic mass extinctions recorded by continental tetrapods from South Africa. *Gondwana Research* **37**:384–396 DOI 10.1016/j.gr.2015.09.008.

Rezende EL, Bacigalupe LD, Nespolo RF, Bozinovic F. 2020. Shrinking dinosaurs and the evolution of endothermy in birds. *Science Advances* **6(1)**:eaaw4486 DOI 10.1126/sciadv.aaw4486.

Ricqlès A de. 1972. Recherches paléohistologiques sur les os longs des tétrapodes III.-Titanosuchiens, Dinocéphales et Dicynodontes. *Annales de Paléontologie* **58**:1–60.

Ricqlès A de. 1976. On bone histology of fossil and living reptiles, with comments on its functional and evolutionary significance. In: Da Bellairs A, Cox CB, eds. *Morphology and biology of reptiles*. London: Academic Press, 123–150.

Ricqlès de A, Meunier FJ, Castanet J, Francillon-Vieillot H. 1991. Comparative microstructure of bone. In: Hall BK, ed. *Bone, Volume 3: Bone matrix and bone specific products*. Boca Raton: CRC Press, 1–77.

Roopnarine PD, Angielczyk KD. 2015. Community stability and selective extinction during the Permian-Triassic mass extinction. *Science* **350(6256)**:90–93 DOI 10.1126/science.aab1371.

Roopnarine PD, Angielczyk KD, Olroyd SL, Nesbitt SJ, Botha-Brink J, Peecook BR, Day MO, Smith RMH. 2018. Comparative ecological dynamics of Permian-Triassic communities from the Karoo, Luangwa, and Ruhuhu basins of southern Africa. *Journal of Vertebrate Paleontology* **37(supl)**:254–272.

Roopnarine PD, Angielczyk KD, Weik A, Dineen A. 2019. Ecological persistence, incumbency and reorganization in the Karoo Basin during the Permian-Triassic transition. *Earth-Science Reviews* **189**:244–263 DOI 10.1016/j.earscirev.2018.10.014.

Ruta M, Angielczyk KD, Fröbisch J, Benton MJ. 2013a. Decoupling of morphological disparity and taxic diversity during the adaptive radiation of anomodont therapsids. *Proceedings of the Royal Society of London B* **280(1768)**:20131071 DOI 10.1098/rspb.2013.1071.

Ruta M, Benton MJ. 2008. Calibrated diversity, tree topology and the mother of mass extinctions: the lesson of temnospondyls. *Palaeontology* **51**:1261–1288 DOI 10.1111/j.1475-4983.2008.00808.x.

Ruta M, Botha-Brink J, Mitchell SA, Benton MJ. 2013b. The radiation of cynodonts and the ground plan of mammalian morphological diversity. *Proceedings of the Royal Society of London B* **280(1769)**:20131865 DOI 10.1098/rspb.2013.1865.

Sander PM, Klein N. 2005. Developmental plasticity in the life history of a prosauropod dinosaur. *Science* **310**:1800–1802 DOI 10.1126/science.1120125.

Sheldon ND, Retallack GJ. 2002. Low oxygen levels in earliest Triassic soils. *Geology* **30(10)**:919–922 DOI 10.1130/0091-7613(2002)030<0919:LOLIET>2.0.CO;2.

Shen S-z, Crowley JL, Wang Y, Bowring SA, Erwin DH, Sadler PM, Cao C-q, Rothman DH, Henderson CM, Ramezani J, Zhang H, Shen Y, Wang X-d, Wang W, Mu L, Li W-z, Tang Y-g, Liu X-l, Liu L-j, Zeng Y, Jiang Y-f, Jin Y-g. 2011.

Calibrating the end-Permian mass extinction. *Science* **334**(**6061**):1367–1372 DOI 10.1126/science.1213454.

Shen J, Yu J, Chen J, Algeo TJ, Xu G, Q F, Shi X, Planavsky NJ, Shu W, Xie S. 2019. Mercury evidence of intense volcanic effects on land during the Permian-Triassic transition. *Geology* **47**(**12**):1117–1121 DOI 10.1130/G46679.1.

Smith RMH, Botha J. 2005. The recovery of terrestrial vertebrate diversity in South African Karoo basin after the End-Permian extinction. *Comptes Rendus Palevol* **4**:555–568.

Smith RMH, Botha-Brink J. 2014. Anatomy of a mass extinction: sedimentological and taphonomic evidence for drought-induced die-offs at the Permian-Triassic boundary in the main Karoo Basin, South Africa. *Palaeogeography, Palaeoclimatology, Palaeoecology* **316**:99–118.

Smith R, Rubidge B, Van der Walt M. 2012. Therapsid biodiversity patterns and paleoenvironments of the Karoo Basin, South Africa. In: Chinsamy-Turan A, ed. *Forerunners of mammals: radiation, histology, biology*. Bloomington: Indiana University Press, 13–64.

Smith RMH, Ward PD. 2001. Pattern of vertebrate extinctions across an event bed at the Permian–Triassic boundary in the Karoo Basin of South Africa. *Geological Society of America Bulletin* **29**:1147–1150.

Song H, Tong J, Chen ZQ. 2011. Evolutionary dynamics of the Permian-Triassic foraminifer size: evidence for Lilliput effect in the end-Permian mass extinction and its aftermath. *Palaeogeography, Palaeoclimatology, Palaeoecology* **308**:98–110 DOI 10.1016/j.palaeo.2010.10.036.

Starck JM, Chinsamy A. 2002. Bone microstructure and developmental plasticity in birds and other dinosaurs. *Journal of Morphology* **254**:232–246 DOI 10.1002/jmor.10029.

Stein K, Prondvai E. 2014. Rethinking the nature of fibrolamellar bone: an integrative biological revision of sauropod plexiform bone formation. *Biological Reviews* **89**:24–47 DOI 10.1111/brv.12041.

Tripathi C, Puri SN. 1962. On the remains of *Lystrosaurus* from the Panchets of the Raniganj coalfield. *Records of the Geological Survey of India* **89**:407–419.

Tripathi C, Satsangi PP. 1963. *Lystrosaurus* fauna of the Panchet series of the Raniganj coalfield. Memoirs of the Geological Survey of India. *Palaeontologia Indica, New series* **37**:1–65.

Twitchett RJ. 2007. The Lilliput effect in the aftermath of the end-Permian extinction event. *Palaeogeography, Palaeoclimatology, Palaeoecology* **252**:132–144 DOI 10.1016/j.palaeo.2006.11.038.

Urbanek A. 1993. Biotic crises in the history of Upper Silurian graptoloids: a palaeobiological model. *Historical Biology: an International Journal of Paleobiology* **7**(**1**):29–50 DOI 10.1080/10292389309380442.

Wall WP. 1983. The correlation between limb-bone density and aquatic habits in recent mammals. *Journal of Vertebrate Paleontology* **57**:197–207.

Ward PD, Botha J, Buick R, De Kock MO, Erwin DH, Garrison GH, Kirschvink JL, Smith R. 2005. Abrupt and gradual extinction among Late Permian land

vertebrates in the Karoo Basin, South Africa. *Science* **307(5710)**:709–714
DOI 10.1126/science.1107068.

Ward PD, Montgomery DR, Smith RMH. 2000. Altered river morphology in South
Africa related to the Permian Triassic extinction. *Science* **289(5485)**:1740–1743
DOI 10.1126/science.289.5485.1740.

Watson DMS. 1912. The skeleton of *Lystrosaurus*. *Records of the Albany Museum*
2:287–299.

Watson DMS. 1913. The limbs of *Lystrosaurus*. *Geological Magazine* **10**:256–258
DOI 10.1017/S0016756800126445.

Whitney MR, Sidor CA. 2020. Evidence of torpor in the tusks of *Lystrosaurus* from the
Early Triassic of Antarctica. *Communications Biology* **3**:471
DOI 10.1038/s42003-020-01207-6.

Wignall PB. 2001. Large igneous provinces and mass extinctions. *Earth-Science Reviews*
53:1–33 DOI 10.1016/S0012-8252(00)00037-4.

Wignall PB, Twitchett RJ. 1996. Oceanic anoxia and the end Permian mass extinction.
Science **272**:1155–1158 DOI 10.1126/science.272.5265.1155.

Xie S, Pancost RD, Yin H, Wang H, Evershed RP. 2005. Two episodes of microbial
change coupled with Permo/Triassic faunal mass extinction. *Nature* **434**:494–497
DOI 10.1038/nature03396.

Yin H, Feng Q, Lai X, Baud A, Tong J. 2007. The protracted Permo-Triassic crisis
and multi-episode extinction around the Permian-Triassic boundary. *Global and
Planetary Change* **55**:1–20 DOI 10.1016/j.gloplacha.2006.06.005.